JOURNAL OF NATURAL PRODUCTS

pubs.acs.org/jnp

Article

An Amphibious Fish-Derived Antimicrobial Peptide, Boleokidin$_{39-61}$, with Broad-Spectrum Antibacterial Activity and In Vivo Protective Efficacy

Yuqi Bai,[1] Jingyuan Zhan,[1] Weibin Zhang, Wenbin Zheng, Fangyi Chen,* and Ke-Jian Wang*

Cite This: https://doi.org/10.1021/acs.jnatprod.5c01507

Read Online

ACCESS | Metrics & More | Article Recommendations | Supporting Information

ABSTRACT: The escalating threat of antimicrobial resistance (AMR) has created an urgent need for alternative therapeutic strategies beyond traditional antibiotics. In this study, we identified a new antimicrobial peptide, Boleokidin$_{39-61}$, encoded by the immune-regulated gene Boleokidin in the amphibious fish *Boleophthalmus pectinirostris*. Notably, the expression of this gene was significantly upregulated in the liver and spleen following *Edwardsiella tarda* infection. Boleokidin$_{39-61}$ exhibited broad-spectrum antibacterial activity against Gram-positive and Gram-negative bacteria, including multidrug-resistant strains. Mechanistic analyses showed that the peptide kills bacteria by disrupting membrane integrity, inhibits biofilm formation, and does not induce resistance under prolonged exposure. Cytotoxicity assays revealed no significant toxicity toward mammalian cells or erythrocytes at antimicrobial concentrations. Importantly, in vivo infection studies using both zebrafish and mice models confirmed the peptide's therapeutic efficacy, demonstrating its ability to reduce bacterial burden and modulate host inflammatory responses. Collectively, these findings highlight Boleokidin$_{39-61}$ as a promising AMP candidate with potent antimicrobial and immunomodulatory properties, offering the potential for application in aquaculture and biomedical fields.

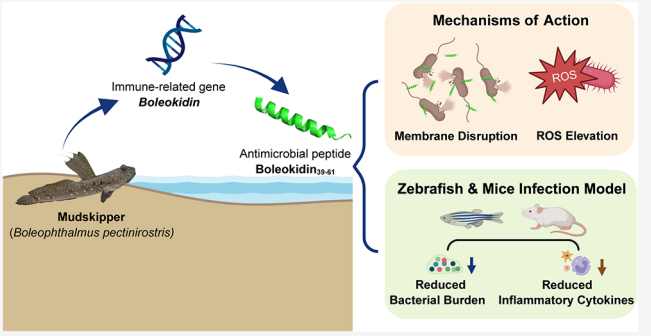

The escalating threat of antibiotic resistance has emerged as a critical issue affecting both global public health and the sustainable development of aquaculture.[1,2] In clinical settings, antibiotic-resistant bacterial infections are associated with prolonged illness, elevated mortality, and significantly increased healthcare costs. According to data from the Centers for Disease Control and Prevention (CDC), antimicrobial-resistant infections affect more than 2.8 million individuals each year in the United States and are responsible for upward of 35,000 fatalities.[3] In aquaculture, widespread and often unregulated antibiotic use—particularly for prophylaxis and growth promotion, has driven the proliferation of resistant bacterial strains. Recent studies have shown that more than 90% of bacterial isolates from aquaculture environments exhibit resistance to at least one antibiotic, with approximately 20% classified as multidrug-resistant.[4]

This situation has prompted researchers to seek novel antimicrobial strategies that can effectively control pathogenic infections while minimizing the development and spread of resistance. In recent years, a range of alternative therapies have been proposed and actively investigated, including vaccines, probiotics, bacteriophage therapy, and AMPs.[5] Among these, AMPs have drawn significant attention due to their broad-spectrum antimicrobial activity, low potential for inducing resistance, and their additional immunomodulatory properties.[6]

AMPs are a class of small, cationic peptides synthesized by a wide variety of organisms, including animals, plants, and microorganisms, serving as key effectors in the innate immune system.[7] Structurally, AMPs can be categorized into α-helical, β-sheet, cyclic, and extended types.[8] They are characterized by rapid bactericidal activity, thermal and proteolytic stability, broad-spectrum action against various pathogens, and a low tendency to induce resistance. The mechanisms by which AMPs exert their antimicrobial effects are diverse. Mechanisms include the direct disruption of microbial membranes via electrostatic interactions and hydrophobic insertion. This process induces pore formation or membrane destabilization, ultimately causing the leakage of intracellular contents.[9] Some AMPs additionally interfere with intracellular processes, such as DNA, RNA, or protein synthesis, or activate host immune responses to enhance pathogen clearance.[10] These multifaceted mechanisms make AMPs promising candidates for combating multidrug-resistant infections.

Received: December 4, 2025
Revised: February 8, 2026
Accepted: February 10, 2026

Table 1. Sequence, Physical, and Chemical Property Information

physicochemical parameters	Boleokidin	Boleokidin$_{39-61}$	LL-37
number of amino acids (aa)	201	23	37
molecular weight (Da)	23346.36	2739.55	4493.32
theoretical pI	10.81	11.47	10.61
molecular formula	$C_{1024}H_{1693}N_{323}O_{279}S_{11}$	$C_{127}H_{228}N_{36}O_{26}S_2$	$C_{205}H_{340}N_{60}O_{53}$
total number of atoms	3330	419	658
grand average of hydropathicity	−0.974	−0.017	−0.724
total hydrophobic ratio	31%	48%	35%
total net charge	+32	+8	+6

Representative AMPs such as human LL-37, frog-derived magainins, bacterially produced nisin, and pig-derived protegrins have demonstrated potential in preclinical and clinical studies. Several AMPs are currently under investigation or in clinical trials for the treatment of diseases such as diabetic foot ulcers, sepsis, bacterial vaginosis, and pneumonia.[11,12]

Marine organisms represent a valuable and largely untapped reservoir of bioactive compounds, including AMPs with unique structural and functional diversity.[13] Adaptation to high salinity, fluctuating temperatures, and complex microbial environments has driven the evolution of highly effective antimicrobial systems in marine species. Among these, the mudskipper *B. pectinirostris*, an amphibious teleost fish inhabiting intertidal mudflats, is of particular interest. Although it does not belong to the amphibians in taxonomy, *B. pectinirostris* encounters both aquatic and terrestrial pathogens due to its amphibious lifestyle, paralleling the ecological pressures faced by true amphibians.[14,15] Notably, amphibians account for a substantial proportion of entries in the Antimicrobial Peptide Database (APD), highlighting their prominent role as a source of diverse AMPs adapted to dual aquatic-terrestrial environments.[16] In addition, the intertidal mudflats inhabited by *B. pectinirostris* are characterized by high microbial loads and complex environmental stressors. Consequently, to survive in such a challenging ecological niche, this species has evolved a robust innate immune system.

Given its unique ecological niche and evolutionary adaptations, *B. pectinirostris* represents a promising candidate for the discovery of novel AMPs. Investigating the antimicrobial repertoire of this species enhances our understanding of innate immune mechanisms in amphibious fishes. Furthermore, they provide a valuable resource for the development of new antimicrobial agents for both clinical and aquaculture settings.

In this study, we utilized a previously established transcriptomic library of *B. pectinirostris* under bacterial infection to investigate the immune response genes. From the differentially expressed genes, we identified a novel AMP gene, herein designated as Boleokidin. Through bioinformatic prediction and experimental validation, we determined that a truncated peptide segment, Boleokidin$_{39-61}$, exhibits potent antimicrobial activity. We further explored its antimicrobial properties and underlying mechanisms, assessed its potential to induce resistance, and conducted safety evaluations. Finally, we validated the in vivo protective efficacy potential of the peptide, using zebrafish and murine infection models. In zebrafish, the peptide demonstrated significant protective efficacy by reducing bacterial load and dampening inflammation. In the murine acute peritonitis model, Boleokidin$_{39-61}$ maintained robust antibacterial activity and effectively suppressed pro-inflammatory cytokines.

RESULTS AND DISCUSSION

Molecular Cloning and Structural Characterization of Boleokidin and Its Antimicrobial Segment Boleokidin$_{39-61}$

Using RACE cloning, we successfully obtained the full-length cDNA sequence of the previously uncharacterized immune-related gene Boleokidin from *B. pectinirostris*. The sequence has been deposited in the GenBank database (accession no. OR195699). As shown in Supporting Figure 1, the cDNA contains a 254 bp 5′ untranslated region (5′UTR), a 387 bp 3′UTR, and an open reading frame encoding a 201-amino-acid precursor protein. Physiochemical prediction indicated that the full-length Boleokidin protein has a molecular mass of ∼23.3 kDa and a theoretical pI of 10.81 (Table 1), suggesting a strongly cationic nature typical of many fish-derived innate immune factors.

Phylogenetic analysis placed Boleokidin within a conserved clade of gobiid fishes, and multiple sequence alignment further confirmed that this gene is relatively conserved among teleost homologs (Figure 1B, C). Despite this overall conservation at the gene level, close inspection of the alignment revealed that the region spanning amino acids 39−61—subsequently designated Boleokidin$_{39-61}$—exhibited variable but functionally relevant divergence among species (Figure 1C, red box).

Comprehensive physicochemical and structural analyses indicate that Boleokidin$_{39-61}$ displays hallmark features of a membrane-active antimicrobial peptide. The several basic residues (e.g., Lys, His) within this region are highly conserved across homologs, conferring a high cationicity[17] with a net charge of +8 (Table 1). Importantly, this 23-aa segment forms a canonical α-helix (Figure 1A), where predicted hydrophobic residues (Val, Leu, Ile) support the formation of an amphipathic surface.[18,19] Collectively, these structural features strongly support its predicted potential as a potent antimicrobial agent.

To further evaluate its antimicrobial potential, Boleokidin$_{39-61}$ was analyzed using three machine-learning algorithms available on the CAMP$_{R4}$ prediction platform.[20] Random forest, support vector machine, and artificial neural network models yielded AMP probability scores of 0.86, 0.99, and 0.98, respectively, consistently classifying this peptide as a putative AMP. These combined structural and computational results identify Boleokidin$_{39-61}$ as a strong candidate antimicrobial domain within the Boleokidin precursor, warranting functional validation in subsequent assays.

Tissue Distribution and Infection-Responsive Expression Dynamics of Boleokidin

To determine the physiological expression profile of Boleokidin under normal conditions, absolute qPCR assays were performed across multiple tissues of healthy *B. pectinirostris* (Figure 2A). Among all examined tissues, the trunk kidney exhibited the highest basal transcript abundance, whereas the liver showed the

https://doi.org/10.1021/acs.jnatprod.5c01507
J. Nat. Prod. XXXX, XXX, XXX−XXX

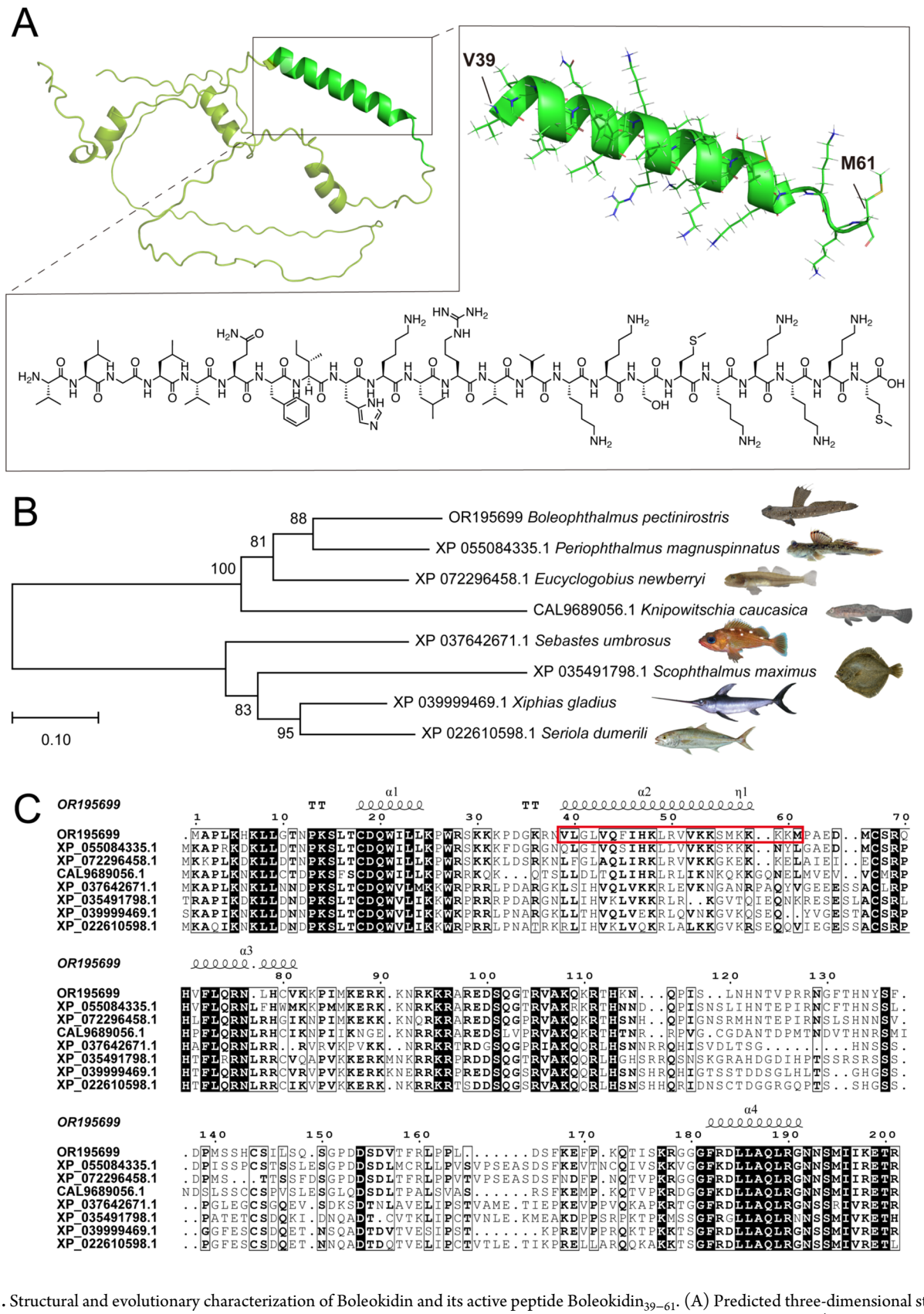

Figure 1. Structural and evolutionary characterization of Boleokidin and its active peptide Boleokidin$_{39-61}$. (A) Predicted three-dimensional structure of the full-length Boleokidin protein generated by AlphaFold, highlighting the antimicrobial peptide segment Boleokidin$_{39-61}$ (amino acids V^{39}-M^{61}) shown as an α-helical structure. The chemical structure of Boleokidin$_{39-61}$ is displayed adjacent to the 3D model and is shown in the neutral form; under physiological conditions, the peptide is expected to carry a net positive charge due to protonation of basic residues. (B) Phylogenetic tree of Boleokidin and homologous sequences from other species constructed using the neighbor-joining method, showing evolutionary relationships and conservation. (C) Multiple sequence alignment of Boleokidin and selected homologs across different species, revealing conserved residues within the antimicrobial domain.

https://doi.org/10.1021/acs.jnatprod.5c01507
J. Nat. Prod. XXXX, XXX, XXX−XXX

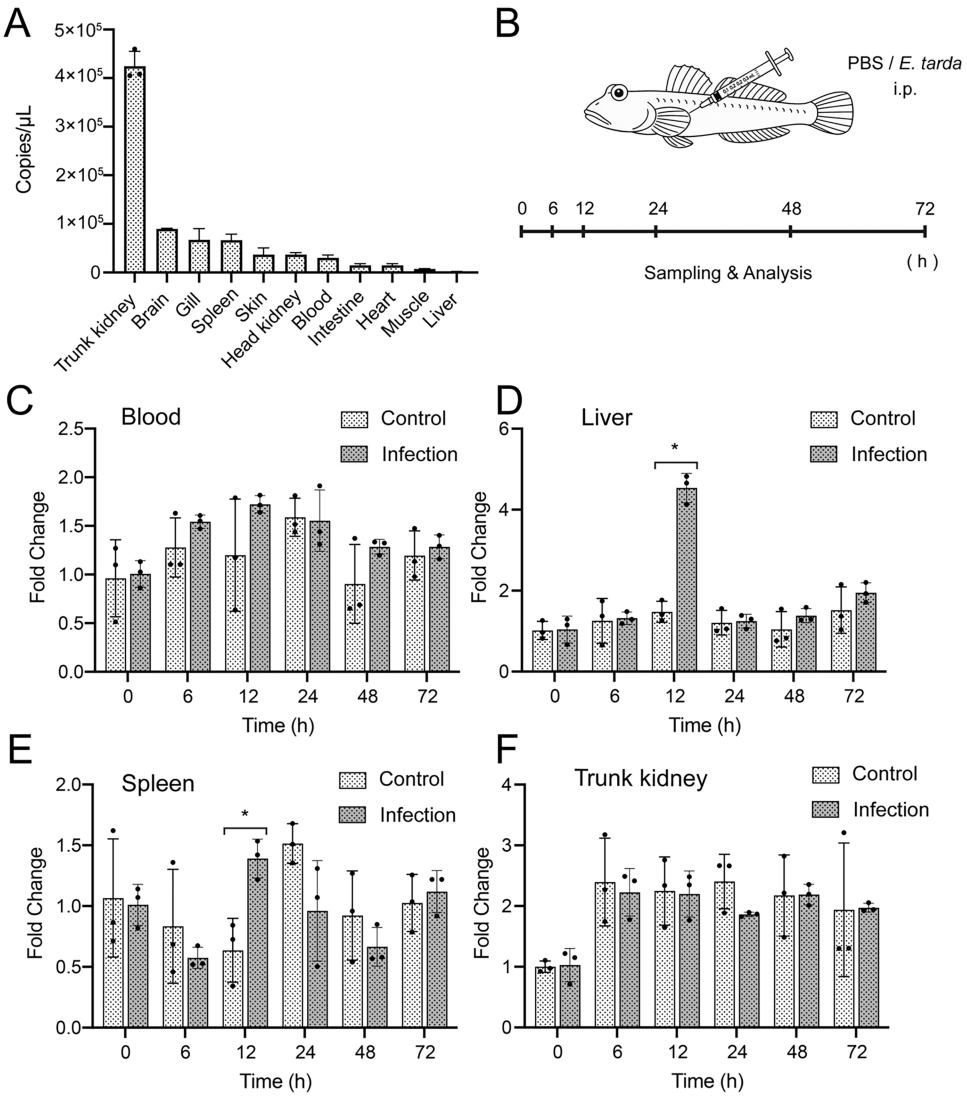

Figure 2. Tissue distribution and infection-induced expression dynamics of the Boleokidin gene in *B. pectinirostris*. (A) Basal expression levels of Boleokidin in various tissues under normal physiological conditions. (B) Schematic timeline of *E. tarda* infection and sample collection at designated time points postinfection. (C−F) Temporal expression profiles of Boleokidin in the blood (C), liver (D), spleen (E), and pronephros (F) following *E. tarda* challenge. Data are presented as fold changes relative to the uninfected control group at 0 h.

lowest level of constitutive expression. Boleokidin is predominantly expressed in the trunk kidney, a key hematopoietic and immune-metabolic organ in teleosts.[21] This localization suggests that the precursor protein may contribute to systemic regulatory functions.

While the liver constitutively produces AMPs like hepcidin (LEAP-1) for iron homeostasis and immunity,[22,23] the low basal expression of Boleokidin points to a distinct, inducible regulatory strategy. Indeed, many inducible AMPs exhibit minimal baseline expression and are rapidly mobilized only upon pathogen exposure.[24,25] This restricted expression profile is characteristic of high-potency effectors, which are transiently upregulated to combat infection but return to baseline to prevent excessive inflammation and tissue damage.[26]

This regulatory pattern was clearly reflected in the infection-challenge experiment. Following *E. tarda* exposure (Figure 2B), the temporal expression dynamics of Boleokidin were analyzed across multiple tissues. In the liver (Figure 2D), a sharp induction peak was observed at 12 h postinfection, with levels significantly elevated compared to uninfected controls. Notably, this induction was rapid and transient, with expression returning to basal levels shortly thereafter. This expression kinetic aligns well with the behavior of inducible AMPs whose primary role is early-pathogen neutralization rather than sustained immune modulation.[27]

A similar transient but pronounced induction was observed in the spleen (Figure 2E), a central lymphoid and hematopoietic organ in teleosts.[28] The surge in spleen-specific expression strongly suggests Boleokidin's involvement in systemic immune activation during early infection. This aligns with the spleen's critical role in coordinating pathogen recognition, leukocyte proliferation, and inflammatory signaling.[29] By contrast, no significant infection-induced fluctuation was observed in the blood or trunk kidneys within the examined time window (Figure 2C, F). This suggests that the rapid hepatic and splenic responses constitute the primary contributors to Boleokidin-mediated immune defense.

Together, these findings indicate that Boleokidin is not a constitutively abundant hepatic AMP like hepcidin but rather an inducible immune effector that responds rapidly to bacterial

https://doi.org/10.1021/acs.jnatprod.5c01507
J. Nat. Prod. XXXX, XXX, XXX−XXX

invasion. Its tissue-specific and time-dependent transcriptional activation highlights its potential role in early antimicrobial defense and immune homeostasis in *B. pectinirostris*.

Antimicrobial Spectrum, Bactericidal Kinetics, and Salt Stability of Boleokidin$_{39-61}$

To experimentally validate the predicted antimicrobial region, the peptide Boleokidin$_{39-61}$ was chemically synthesized according to its amino-acid sequence identified from the Boleokidin precursor protein.

The antimicrobial properties of Boleokidin$_{39-61}$ were evaluated against a broad panel of microorganisms including Gram-positive bacteria, Gram-negative bacteria, fungi, and clinically isolated multidrug-resistant (MDR) strains. As summarized in Table 2, the peptide exhibited marked and broad-spectrum inhibitory activity, with MIC values comparable to or lower than those of the human cathelicidin-derived AMP LL-37. Boleokidin$_{39-61}$ exhibited potent activity against a broad spectrum of bacteria, notably including multidrug-resistant (MDR) isolates such as *Acinetobacter baumannii*, *Pseudomonas aeruginosa*, and MRSA. This robust efficacy suggests that the peptide likely exerts its activity through membrane-targeting mechanisms, thereby circumventing classical resistance processes such as efflux, target modification, or enzymatic inactivation.[30]

Table 2. Broad-Spectrum Antimicrobial Assay for Boleokidin$_{39-61}$

strains	CGMCC No.[a]	MIC[b] (μM)	MBC/MFC	MIC
gram-negative bacteria	Boleokidin$_{39-61}$			**LL-37**
A. baumannii	1.6769	1.5−3	1.5−3	3−6
P. aeruginosa	1.2421	3−6	6−12	6−12
E. coli	1.2385	6−12	6−12	12−24
A. hydrophila	1.2017	12−24	24−48	48−96
E. tarda	1.1872	12−24	24−48	>96
Vibrio alginolyticus	1.1833	6−12	12−24	12−24
gram-positive bacteria	Boleokidin$_{39-61}$			LL-37
Staphylococcus aureus	1.2465	3−6	6−12	12−24
Staphylococcus epidermidis	1.4260	<1.5	1.5−3	3−6
Listeria monocytogenes	1.10753	3−6	3−6	1.5−3
Enterococcus faecalis	1.2135	3−6	3−6	6−12
Corynebacterium glutamicum	1.1886	<1.5	<1.5	<1.5
Bacillus cereus	1.3760	6−12	6−12	<1.5
Fungi	Boleokidin$_{39-61}$			LL-37
Cryptococcus neoformans	2.1563	<1.5	<1.5	1.5−3
Candida albicans	2.2411	12−24	12−24	6−12
Fusarium oxysporum	3.6785	12−24	12−24	12−24
Fusarium solani	3.5840	12−24	12−24	6−12
Aspergillus flavus	3.4410	12−24	24−48	12−24
MDR Strains[c]	Boleokidin$_{39-61}$			LL-37
A. baumannii-QZ18050	-	1.5−3	1.5−3	3−6
A. baumannii-QZ18055	-	3−6	3−6	6−12
P. aeruginosa-QZ19121	-	3−6	6−12	6−12
P. aeruginosa-QZ19122	-	1.5−3	3−6	6−12
MRSA-QZ19130	-	3−6	6−12	12−24
MRSA-QZ19134	-	3−6	3−6	12−24

[a]Strain accession numbers refer to the entries in the China General Microbiological Culture Collection Center. [b]Antimicrobial results are presented in the A-B format, where A indicates the highest concentration showing visible microbial growth and B denotes the lowest concentration at which growth was completely inhibited. [c]Multidrug-resistant clinical isolates were obtained from the Second Affiliated Hospital of Fujian Medical University (Quanzhou, Fujian, China).

In contrast to its strong antibacterial activity, the peptide showed moderate antifungal effects, primarily reflected in the inhibition of fungal spore germination (Supporting Figure 2). This differential activity may stem from the substantial structural differences between bacterial membranes and fungal cell walls. Fungal cells possess a thick, multilayered wall composed of chitin, β-glucans, and mannoproteins. This complex structure functions as a physical and chemical barrier, restricting peptide diffusion and promoting nonspecific sequestration.[31] As a result, the effective concentration of Boleokidin$_{39-61}$ reaching the fungal plasma membrane is likely reduced, leading to diminished inhibitory activity relative to bacteria.

Given the promising antimicrobial spectrum, we further assessed the bactericidal kinetics of Boleokidin$_{39-61}$ using *A. baumannii* as a representative pathogen. As shown in Figure 3A, the peptide demonstrated rapid killing activity, eliminating over 90% of viable bacteria within 20 min at 1× MBC. At 2× MBC, a comparable level of killing occurred within only 10 min, highlighting the peptide's fast-acting bactericidal mode, which is a desirable property for therapeutic candidates targeting acute infections.

Salt tolerance is another important parameter that influences the practical applicability of AMPs. The activity of many natural AMPs is attenuated under physiologically relevant ionic strengths due to charge shielding or disrupted peptide−membrane interactions.[32] In contrast, Boleokidin$_{39-61}$ retained robust antibacterial activity under Na^+ concentrations of up to 80 mM (Figure 3B), indicating relatively low salt sensitivity. This characteristic suggests that the peptide can maintain functional integrity in freshwater or low-salinity aquaculture environments, as well as in human tissues such as skin and mucosal surfaces, where ionic strength is moderate. Moreover, its stability under low-salt conditions enhances its potential utility in food preservation, antimicrobial coatings, and hydrogel-based delivery systems, expanding its application prospects as an alternative to conventional antibiotics.

Collectively, these findings demonstrate that Boleokidin$_{39-61}$ possesses a broad antimicrobial spectrum, rapid bactericidal kinetics, and robust salt stability. These attributes establish it as a promising membrane-active peptide with significant potential for biomedical, aquaculture, and biotechnological applications.

Membrane-Disruptive Mechanism of Boleokidin$_{39-61}$

To elucidate the bactericidal mode of action of Boleokidin$_{39-61}$, we examined its effects on bacterial membrane integrity using CLSM- and scanning electron microscope (SEM)-based assays. For mechanistic investigations, *A. baumannii* and *S. aureus* were selected as representative Gram-negative and Gram-positive pathogens, respectively. This choice was based on the World Health Organization (WHO) designation of these species as members of the clinically critical ESKAPE group, reflecting their high relevance in multidrug-resistant infections. Thus, using these two pathogens provides a clinically meaningful model for evaluating membrane-disruptive mechanisms.

CLSM analysis using SYTO 9/PI staining revealed a pronounced increase in the number of PI-positive cells following peptide treatment. This result indicates that Boleokidin$_{39-61}$ rapidly compromises bacterial inner membrane permeability in both *A. baumannii* and *S. aureus* (Figure 3D). Consistent with

https://doi.org/10.1021/acs.jnatprod.5c01507
J. Nat. Prod. XXXX, XXX, XXX−XXX

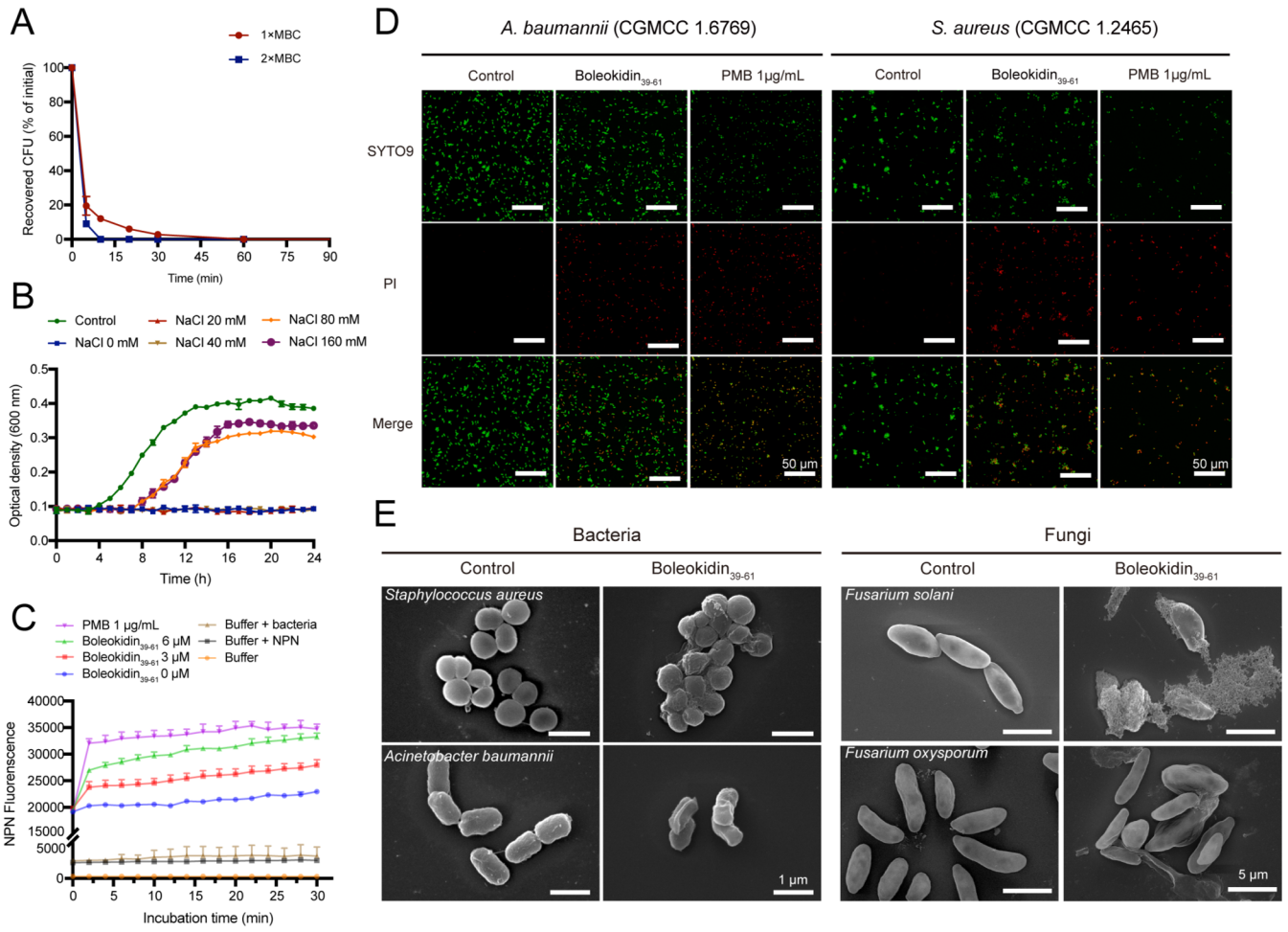

Figure 3. Antimicrobial kinetics, salt stability, and structural effects of Boleokidin$_{39-61}$ on bacterial cells. (A) Time-kill kinetics of *A. baumannii* following treatment with Boleokidin$_{39-61}$ at 1× and 2 × MBC. (B) Evaluation of salt stability of Boleokidin$_{39-61}$ under increasing concentrations of sodium ions (Na^+). (C) Effects of Boleokidin$_{39-61}$ on the outer membrane permeability of *A. baumannii* assessed by the NPN uptake assay. (D) Analysis of bacterial membrane permeabilization using CLSM with SYTO 9/PI staining. (E) SEM analysis of bacterial and fungal spores ultrastructure after peptide treatment.

these findings, SEM imaging revealed severe morphological damage, characterized by surface collapse, membrane shrinkage, and pore-like disruptions (Figure 3E). These observations confirm that the peptide exerts potent membrane-disruptive effects.

Given that PI uptake primarily reflects inner membrane permeabilization, we further evaluated whether Boleokidin$_{39-61}$ also affects the outer membrane of Gram-negative bacteria. To this end, we performed an NPN fluorescence assay, a widely used method to monitor disruptions in outer membrane integrity.[33] As shown in Figure 3C, Boleokidin$_{39-61}$ caused a dose-dependent increase in NPN fluorescence, demonstrating the enhanced accessibility of the hydrophobic NPN probe to the lipid-rich core of the outer membrane. This result indicates that the peptide significantly compromises the outer membrane barrier prior to inner membrane damage and thus facilitates deeper membrane insertion and subsequent bactericidal action. The sequential disruption of both the outer and inner membranes is consistent with the behavior of amphipathic α-helical AMPs that destabilize Gram-negative envelopes through progressive membrane partitioning.

Structurally, Boleokidin$_{39-61}$ is a short, amphipathic α-helical peptide carrying a net positive charge of +8. This unique physicochemical profile, characterized by cationic residues clustered on the polar face of the helix, promotes rapid binding to the negatively charged LPS or LTA on bacterial surfaces.[34−36] Upon establishing this surface anchoring, the peptide leverages its amphipathic α-helical structure to penetrate deeply into the lipid bilayer interface.[37,38] This dual organization of the peptide enables a strong membrane-partitioning effect, which is a defining feature of potent α-helical AMPs.[39] Cationic AMPs accumulate on membranes with partition coefficients approaching 10^4, allowing low micromolar bulk concentrations to reach millimolar surface levels.[40] This dense clustering induces membrane thinning, curvature stress, and pore formation, ultimately destabilizing the bilayer.

Taken together, the CLSM/SEM evidence and physicochemical properties support a stepwise mechanism. Specifically, Boleokidin$_{39-61}$ initially binds LPS or LTA via electrostatic attraction, followed by amphipathic helix insertion and high-density accumulation at the membrane interface. This process induces mechanical disruption, pore formation, and ultimately the loss of cellular integrity, establishing membrane destabilization as the primary mechanism underlying the potent antibacterial activity of Boleokidin$_{39-61}$.

https://doi.org/10.1021/acs.jnatprod.5c01507
J. Nat. Prod. XXXX, XXX, XXX−XXX

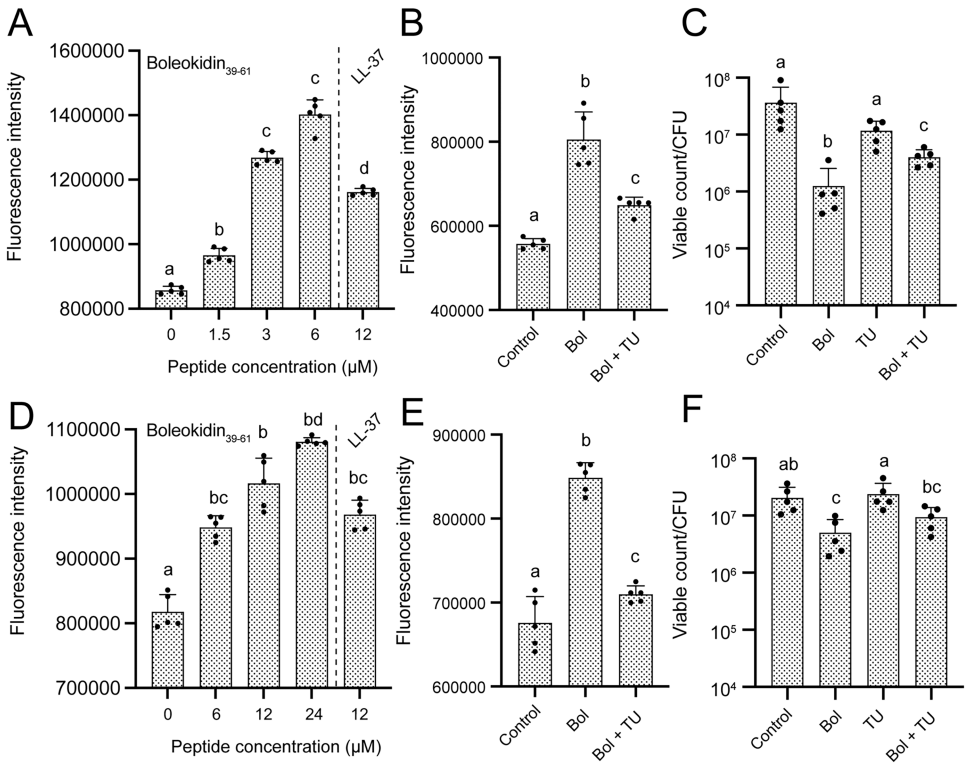

Figure 4. Intracellular ROS generation and the contribution of ROS to Boleokidin$_{39-61}$-mediated bacterial killing. (A) ROS production in *A. baumannii* after treatment with Boleokidin$_{39-61}$. (B) ROS levels in *A. baumannii* treated with Boleokidin$_{39-61}$ (Bol) alone or together with thiourea (TU). (C) Effects of thiourea on the antibacterial activity of Boleokidin$_{39-61}$ in *A. baumannii*. (D) ROS production in *S. aureus* after treatment with Boleokidin$_{39-61}$. (E) ROS levels in *S. aureus* treated with Boleokidin$_{39-61}$ alone or together with thiourea. (F) Effects of thiourea on the antibacterial activity of Boleokidin$_{39-61}$ in *S. aureus*.

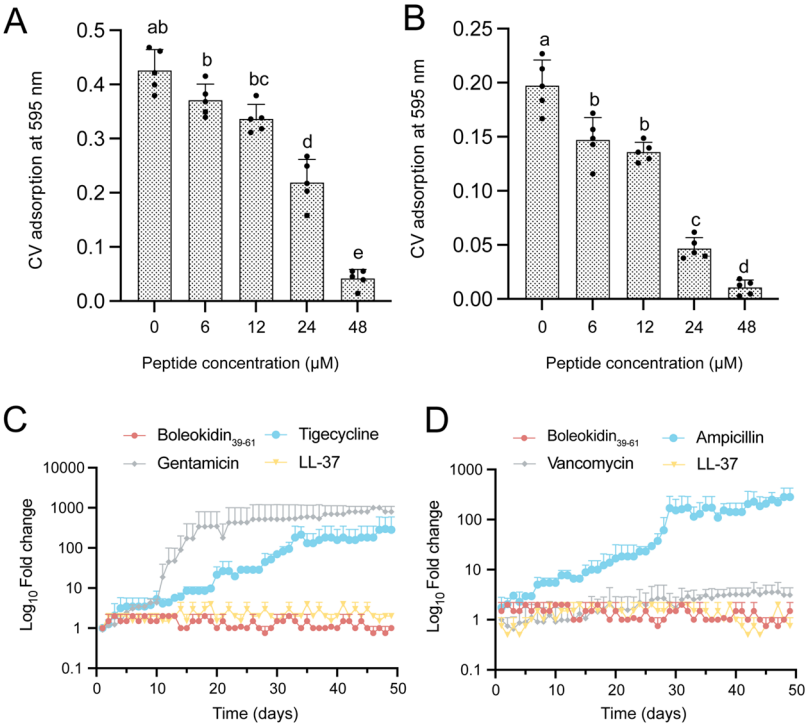

Figure 5. Inhibitory effects of Boleokidin$_{39-61}$ on biofilm formation and resistance development. (A, B) Inhibition of biofilm formation in *A. baumannii* (A) and *S. aureus* (B) following treatment with Boleokidin$_{39-61}$. (C, D) Long-term resistance development assays showing the MIC trajectories of *A. baumannii* (C) and *S. aureus* (D) during 48 consecutive days of daily exposure to sub-MIC levels of Boleokidin$_{39-61}$ and reference antimicrobials.

https://doi.org/10.1021/acs.jnatprod.5c01507
J. Nat. Prod. XXXX, XXX, XXX−XXX

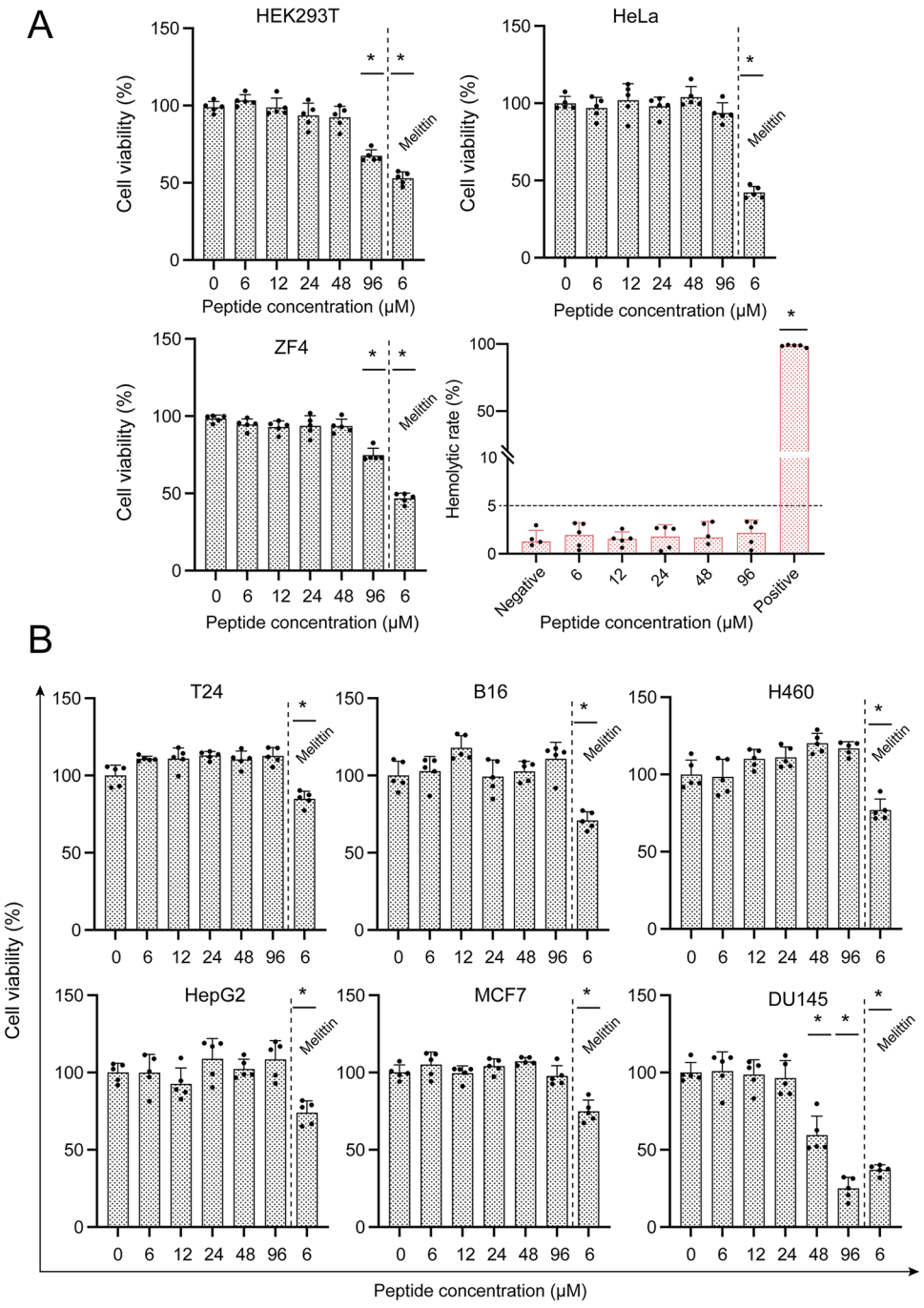

Figure 6. Cytotoxicity and hemolytic activity evaluation of Boleokidin$_{39-61}$. (A) Cytotoxic effects of Boleokidin$_{39-61}$ at varying concentrations on HEK293T, HeLa, and ZF4 cells, along with hemolytic activity assessed using mouse erythrocytes. Cell viability was measured via MTS assay, and hemolysis was quantified by spectrophotometric analysis of hemoglobin release. (B) Cytotoxicity profiling of Boleokidin$_{39-61}$ in additional human cancer cell lines, including T24, B16, H460, HepG2, MCF7, and DU145.

Boleokidin$_{39-61}$-Induced Bacterial Damage Inhibits Biofilm Formation and Minimizes Resistance Development

To gain a further understanding of the bactericidal mode of action of Boleokidin$_{39-61}$, we examined intracellular ROS production, biofilm inhibition, and long-term resistance development. In parallel with membrane permeabilization, Boleokidin$_{39-61}$ induced a strong and dose-dependent increase in intracellular ROS levels in both *A. baumannii* and *S. aureus* (Figure 4A, D). To assess the contribution of ROS to the bactericidal process, thiourea (TU) (a well-characterized scavenger of hydroxyl radicals ($^{\bullet}$OH)[41]) was applied prior to peptide treatment. TU significantly attenuated the ROS surge induced by Boleokidin$_{39-61}$ in both bacterial species (Figure 4B, E), although residual DCF fluorescence remained higher than that of the untreated control. This suggests that part of the ROS signal likely originates from H_2O_2/peroxidase-driven oxidation reactions, which TU does not effectively neutralize.

We next assessed whether ROS scavenging influences bacterial viability. TU treatment alone did not significantly affect the viable counts of either species. However, in *A. baumannii* (Figure 4C), TU treatment significantly restored bacterial viability compared to the peptide-only group,

https://doi.org/10.1021/acs.jnatprod.5c01507
J. Nat. Prod. XXXX, XXX, XXX−XXX

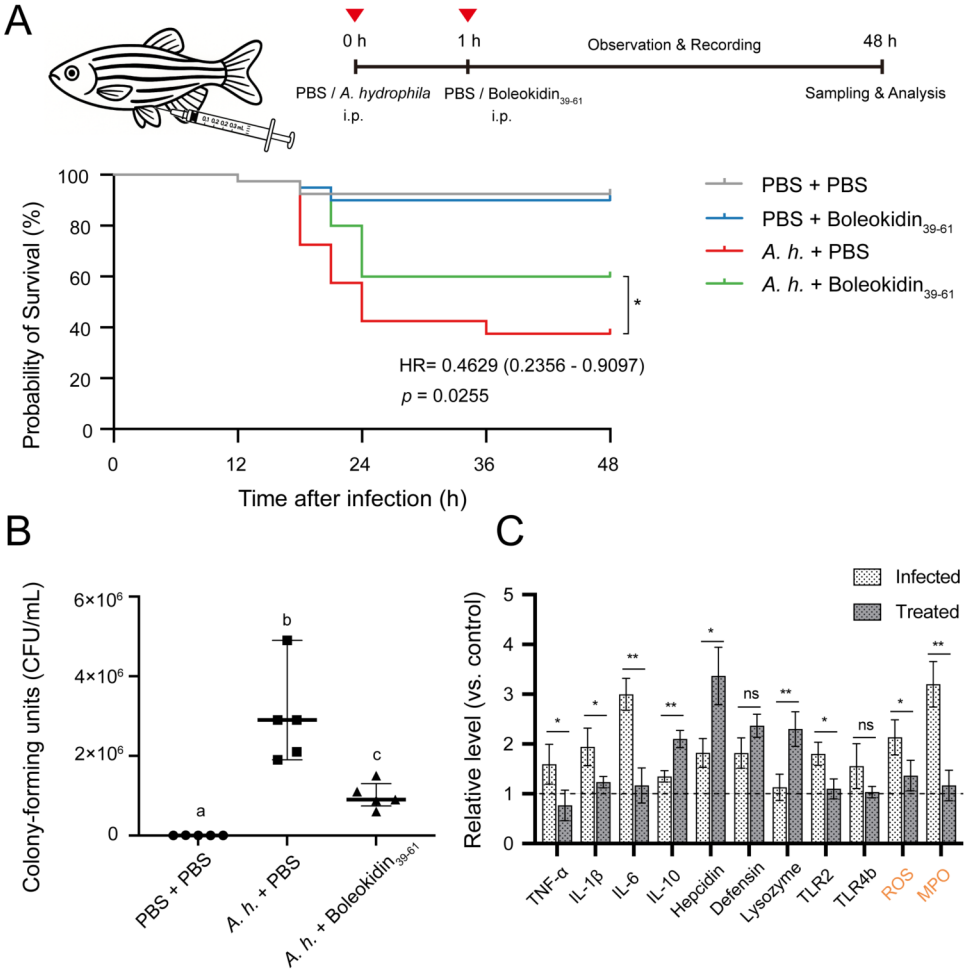

Figure 7. Immunoprotective effects of Boleokidin$_{39-61}$ in zebrafish challenged with *A. hydrophila*. (A) Experimental timeline schematic and Kaplan−Meier survival curves depicting zebrafish survival over a 48-h postinfection period with or without peptide treatment. (B) Quantification of bacterial load in liver tissues 48 h after infection, measured to assess the efficacy of Boleokidin$_{39-61}$ in reducing pathogen burden. (C) Relative expression levels of immune-related genes, as well as ROS levels and MPO activity in liver samples. Data are normalized to the uninfected control group and presented as fold changes.

demonstrating that ROS-mediated damage contributes to but does not solely determine the bactericidal outcome. Importantly, substantial killing activity remained even in the presence of TU, indicating that Boleokidin$_{39-61}$ primarily relies on its membrane-disruptive mechanism, with ROS serving as an amplifying component of cellular damage. In contrast, no significant rescue of survival was observed in *S. aureus* (Figure 4F), which may reflect species-specific oxidative stress responses. The *S. aureus* is known to employ diverse protective strategies—including endogenous antioxidant production and redox metabolic adjustments—to mitigate oxidative injury, and ROS can even trigger phenotypic states associated with antibiotic tolerance.[42,43] These differences likely account for the weaker TU-mediated rescue of this species.

Given that biofilms provide critical protection for bacteria against antimicrobial agents and immune clearance, we assessed whether Boleokidin$_{39-61}$ could interfere with biofilm formation. As shown in Figure 5A,B, the peptide exhibited a robust, dose-dependent inhibition of biofilm formation in both Gram-negative and Gram-positive species. This effect is likely attributable to the early membrane damage caused by the peptide, which disrupts bacterial adhesion, surface sensing, and quorum-sensing-associated signaling—key processes required for initial biofilm establishment.[44,45] Additionally, ROS elevation may contribute to biofilm suppression, as oxidative stress can inhibit extracellular polymeric substance (EPS) synthesis and impair the metabolic stability required for microcolony maturation.[46] Together, these findings indicate that Boleokidin$_{39-61}$ not only eradicates planktonic bacteria but also effectively counters the formation of persistent biofilm communities.

A critical evaluation of antimicrobial candidates involves assessing the potential for resistance development.[47] To address this, we performed a 48-day serial passaging experiment using sub-MIC concentrations of Boleokidin$_{39-61}$ and compared its resistance trajectory with those of conventional antibiotics. For *A. baumannii*, gentamicin treatment rapidly led to >100-fold MIC elevation, and tigecycline showed gradual but evident MIC increases over time (Figure 5C). Similarly, in *S. aureus*, ampicillin induced rapid resistance development, and vancomycin caused a moderate MIC elevation (Figure 5D). In striking contrast, Boleokidin$_{39-61}$ did not induce any significant MIC change throughout the entire 48-day study, mirroring the resistance-refractory behavior of the host-derived AMP LL-37.

The failure of bacteria to develop resistance against Boleokidin$_{39-61}$ likely reflects the fundamental physical nature

https://doi.org/10.1021/acs.jnatprod.5c01507
J. Nat. Prod. XXXX, XXX, XXX−XXX

of its bactericidal mechanism. Membrane-targeting peptides act directly on the lipid bilayer rather than on enzymatic or protein targets, leaving bacteria with limited evolutionary routes to escape killing. Alterations that significantly modify membrane charge or lipid composition often incur high fitness costs; therefore, resistance to α-helical AMPs rarely emerges in natural systems.[48] Furthermore, the peptide's ability to inhibit biofilm formation eliminates another major reservoir for adaptive resistance, as biofilms often serve as incubators for mutational events and horizontal gene transfer.[49]

Collectively, these findings indicate that Boleokidin$_{39-61}$ exerts potent antibacterial effects through a dual mechanism: primary membrane disruption coupled with ROS-mediated secondary damage. Although ROS contributes to the killing process—particularly in *A. baumannii*, the persistence of substantial bactericidal activity under ROS-scavenging conditions underscores the dominant role of membrane targeting. The peptide's robust antibiofilm activity and minimal propensity for resistance development further highlight its promise as a next-generation antimicrobial agent.

Cytotoxicity and Hemocompatibility of Boleokidin$_{39-61}$

The biosafety profile of Boleokidin$_{39-61}$ was assessed using mammalian cell lines and mouse erythrocytes to evaluate potential adverse effects at therapeutically relevant concentrations. As shown in Figure 6A, the peptide exhibited minimal cytotoxicity toward HEK293T, HeLa, and ZF4 cells across a wide concentration range. Cell viability remained largely unaffected at concentrations corresponding to its antimicrobial MIC and MBC values, with only a moderate decline observed at the highest tested concentration (96 μM). This low cytotoxicity is consistent with the structural selectivity of cationic α-helical AMPs, which preferentially target negatively charged bacterial membranes over the zwitterionic phospholipid-rich membranes of mammalian cells.[50]

Hemocompatibility was further validated using freshly isolated mouse red blood cells. Boleokidin$_{39-61}$ showed no detectable hemolytic activity at any of the tested concentrations (Figure 6A), indicating that the peptide does not perturb erythrocyte membranes, even at supraphysiological levels. The absence of hemolysis highlights the peptide's favorable safety profile and distinguishes it from many membrane-active AMPs whose clinical utility is limited by erythrocyte lysis.[51]

To further characterize the peptide's selectivity toward mammalian cells, we evaluated its cytotoxic activity against six human cancer cell lines. As shown in Figure 6B, Boleokidin$_{39-61}$ exhibited selective cytotoxicity toward the DU145 prostate cancer cell line, whereas other cancer cell lines (T24, B16, H460, HepG2, and MCF7) remained largely unaffected. This selective sensitivity likely stems from specific variations in the membrane composition of DU145 cells, such as increased exposure of anionic phosphatidylserine, reduced cholesterol content, and altered fluidity.[52] Collectively, these features enhance the susceptibility to membrane-active peptides. Although preliminary, these observations raise the possibility that Boleokidin$_{39-61}$ may possess dual antibacterial and anticancer potential, warranting further mechanistic and functional studies in tumor-selective membrane targeting.

Overall, the low cytotoxicity, absence of hemolysis, and cell-type-specific membrane susceptibility demonstrate that Boleokidin$_{39-61}$ has a favorable safety window suitable for therapeutic development. The clear selectivity for bacterial membranes reinforces its potential as a promising antimicrobial candidate with minimal risk to host cells.

Immunoprotective Effects of Boleokidin$_{39-61}$ in a Zebrafish Infection Model

To evaluate the in vivo protective efficacy of Boleokidin$_{39-61}$, a zebrafish infection model was established using *Aeromonas hydrophila*—a well-characterized Gram-negative pathogen widely used in teleost immunology. Unlike *E. tarda*, whose infection dynamics in zebrafish can vary substantially between strains and laboratories, *A. hydrophila* induces a reproducible acute infection suitable for standardized assessment of survival, inflammatory markers, and oxidative stress responses.[53] The use of *A. hydrophila* therefore complements the *E. tarda*-based discovery in *B. pectinirostris*, enabling a broader evaluation of the peptide's biological relevance.

As shown in Figure 7A, administration of Boleokidin$_{39-61}$ significantly improved zebrafish survival following bacterial challenge, resulting in a 22.5% increase in survival compared to the infected control group. Kaplan−Meier analysis further confirmed the statistical significance of this protective effect (p = 0.0255). Consistent with the survival data, the Cox proportional hazards model demonstrated that peptide treatment substantially mitigated infection-induced mortality risk (hazard ratio: 0.4629; 95% CI: 0.2356−0.9097). Specifically, Boleokidin$_{39-61}$ reduced the risk of death by approximately 54%.

The liver serves as the core organ of innate immunity in teleost fish, acting as the primary site for synthesizing acute-phase proteins and complement factors during infections.[54] Therefore, we analyzed the bacterial burden, gene expression, and markers of oxidative stress in the liver to evaluate the regulatory effects of Boleokidin$_{39-61}$ on immune responses.

The bacterial load assessment (Figure 7B) revealed that Boleokidin$_{39-61}$ treatment significantly reduced the hepatic bacterial burden in zebrafish compared to the control group. This finding indicates that the peptide retains its potent bactericidal activity, even within the complex physiological environment of the host, thereby directly limiting pathogen proliferation.

Furthermore, the peptide exerts a crucial immunomodulatory effect. We observed a significant suppression of pro-inflammatory cytokines (TNF-α, IL-1β, IL-6) alongside an upregulation of the anti-inflammatory cytokine IL-10 (Figure 7C). These changes suggest that Boleokidin$_{39-61}$ actively mitigates infection-induced immunopathology. Additionally, treatment enhanced the expression of innate immune effectors, such as hepcidin and lysozyme, while also increasing TLR2 expression. This implies reinforcement of host immune signaling. Moreover, oxidative stress markers (ROS levels and MPO activity) were significantly reduced in the peptide-treated group (Figure 7C), indicating relief from oxidative injury. These results collectively suggest that by dampening excessive inflammatory responses and oxidative stress Boleokidin$_{39-61}$ protects host tissues from collateral damage, thereby contributing to the observed enhanced survival rates observed.

In summary, these findings demonstrate that Boleokidin$_{39-61}$ provides multifaceted immunoprotective activity in vivo, combining direct bacterial clearance with the suppression of inflammatory and oxidative stress responses. The significant reduction in mortality risk further underscores its potential as an effective antimicrobial and immunomodulatory peptide.

https://doi.org/10.1021/acs.jnatprod.5c01507
J. Nat. Prod. XXXX, XXX, XXX−XXX

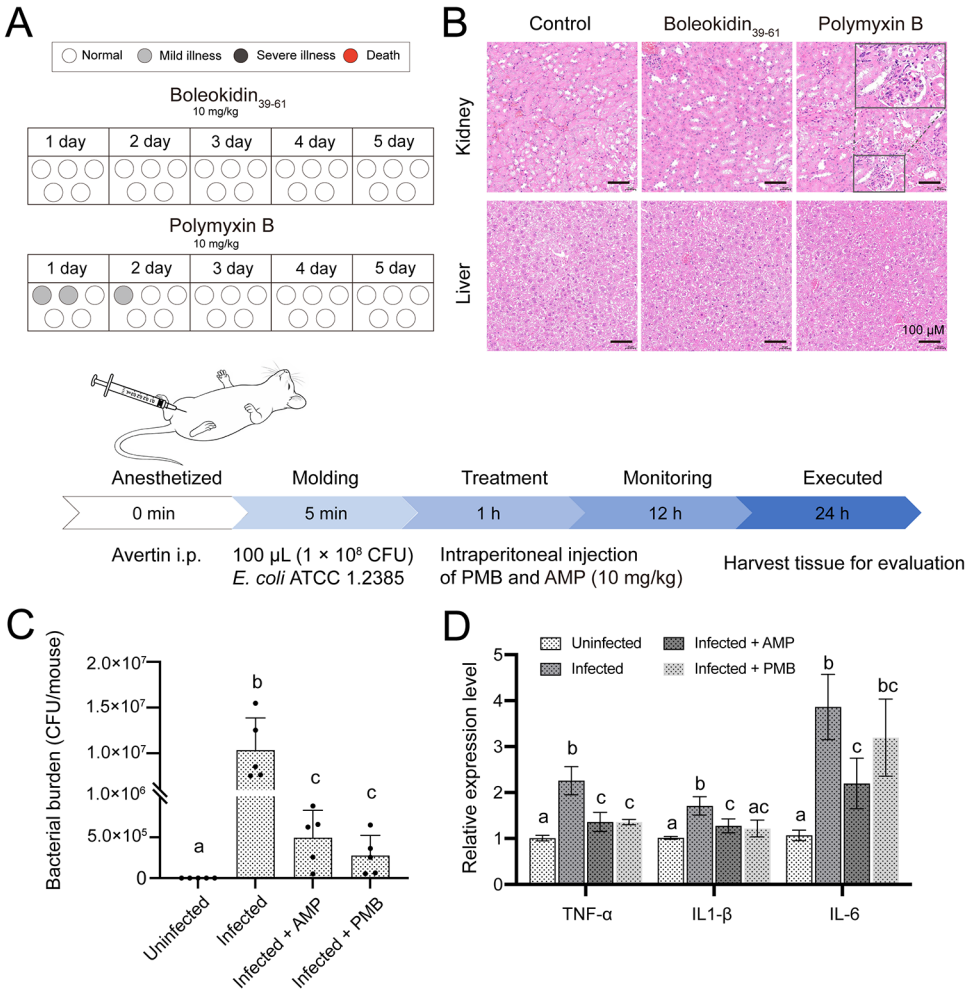

Figure 8. Safety evaluation and therapeutic efficacy of Boleokidin$_{39-61}$ in a mouse acute peritonitis model. (A) Clinical observations during the toxicity assessment. (B) Representative H&E-stained liver and kidney sections from the toxicity study. (C) Hepatic bacterial loads after *E. coli* infection and treatment. (D) Hepatic expression of TNF-α, IL-1β, and IL-6 measured by qPCR.

Therapeutic Efficacy of Boleokidin$_{39-61}$ in a Mice Acute Peritonitis Model

In the acute toxicity assessment, intraperitoneal administration of Boleokidin$_{39-61}$ at 10 mg/kg did not induce any observable adverse effects in mice during the 5-day monitoring period (Figure 8A). All five animals exhibited normal activity, and no signs of mild or severe illness were recorded. Histopathological examination further confirmed the absence of noticeable tissue alterations in the liver and kidney sections from Boleokidin$_{39-61}$-treated mice (Figure 8B). In contrast, mice receiving Polymyxin B at the same dosage exhibited transient mild illness during the first 2 days. Histological analysis further revealed mild inflammatory cell aggregation in kidney tissue, a finding consistent with the antibiotic's known nephrotoxicity.[55] These observations indicate that Boleokidin$_{39-61}$ is well tolerated at 10 mg/kg with no detectable acute organ toxicity under the tested conditions.

In the *E. coli*-induced acute peritonitis model, both Boleokidin$_{39-61}$ and Polymyxin B significantly reduced hepatic bacterial burden 24 h after treatment compared with infected controls (Figure 8C), demonstrating potent in vivo antibacterial activity. Analysis of inflammatory cytokines revealed that Boleokidin$_{39-61}$ markedly decreased TNF-α, IL-1β, and IL-6 expression relative to the infected controls (Figure 8D). Polymyxin B produced similar reductions in TNF-α and IL-1β, with IL-1β approaching baseline levels. However, IL-6 levels in the Polymyxin B-treated group did not show a statistically significant decrease despite the marked reduction in bacterial load. This discrepancy may reflect the drug's intrinsic cytotoxic effects, which have been reported to trigger stress-related cytokine responses independently of bacterial burden.[56] The mild renal inflammation observed in the toxicity assessment further supports the possibility that Polymyxin B-associated tissue stress could sustain IL-6 expression, thereby masking the expected inflammatory decline following bacterial clearance.

Taken together, these findings demonstrate that Boleokidin$_{39-61}$ displays a favorable safety profile at the tested dose and exerts strong antibacterial and anti-inflammatory effects in vivo, comparable to those of Polymyxin B. The peptide's ability to reduce bacterial load and modulate inflammatory cytokines highlights its therapeutic potential, while future optimization of dosing or delivery strategies may further enhance its applicability in mammalian systems.

Final Summary and Implications

The accelerating global spread of antimicrobial resistance poses a major threat to public health and aquaculture, underscoring the urgent need for therapeutics that circumvent traditional antibiotic targets. Antimicrobial peptides offer clear advantages

https://doi.org/10.1021/acs.jnatprod.5c01507
J. Nat. Prod. XXXX, XXX, XXX−XXX

in this context: their rapid, membrane-directed killing, broad pathogen coverage, and low propensity for resistance development distinguish them from conventional antibiotics.

In this study, we characterized Boleokidin$_{39-61}$, an α-helical peptide derived from *B. pectinirostris*. The peptide exhibited potent antibacterial activity characterized by rapid bactericidal kinetics and robust membrane-disruptive properties. Notably, it also effectively inhibited biofilm formation and maintained its efficacy against multidrug-resistant strains. The peptide demonstrated excellent biosafety in vitro and maintained stable antimicrobial activity under physiological conditions. Importantly, in vivo studies using both zebrafish and mice infection models confirmed its therapeutic efficacy, with Boleokidin$_{39-61}$ reducing the bacterial burden and mitigating excessive inflammatory responses in both systems. These results collectively demonstrate that Boleokidin$_{39-61}$ confers broad in vivo protection and possesses dual antimicrobial and immunomodulatory functions.

Together, these findings highlight Boleokidin$_{39-61}$ as a promising antimicrobial candidate with distinct advantages over traditional antibiotics. Consequently, it represents a viable alternative strategy for combating resistant pathogens and advances the development of AMP-based therapeutics.

EXPERIMENTAL SECTION

Biological Materials

Adult *B. pectinirostris* (body length: 12 ± 1 cm; body weight: 30 ± 3 g) were obtained from an aquaculture farm in Ningde, Fujian Province, China. Prior to experimentation, fish were acclimated for 1 week in a recirculating aquaculture system maintained at 26 °C and 10‰ salinity. Tissues collected for analysis included blood, spleen, head kidney, trunk kidney, gill, skin, heart, liver, muscle, intestine, and brain. Adult zebrafish (*Danio rerio*) AB strains (body length: 3 ± 0.5 cm; body weight: 0.5 ± 0.1 g) were purchased from the China Zebrafish Resource Center (Wuhan, China) and maintained in a temperature-controlled recirculating water system at 26 °C. Fish were fed brine shrimp twice daily (morning and evening) and fasted for 24 h prior to experiments. All fish were anesthetized using MS-222 (200 mg/L ethyl 3-aminobenzoate methanesulfonate, Sigma-Aldrich) before injection or dissection. All animal experiments were approved by the Animal Ethics Committee of Xiamen University.

The ZF4 zebrafish fibroblast cell line was obtained from the China Zebrafish Resource Center (http://www.zfish.cn/). The HEK293T human embryonic kidney cell line and all cancer cell lines used in this study were purchased from the Chinese Academy of Sciences Cell Bank (https://www.cellbank.org.cn/). Cells were cultured in DMEM/F-12, RPMI-1640, or DMEM medium (Gibco) supplemented with 10% fetal bovine serum (FBS) and 1% penicillin-streptomycin (Gibco), and incubated at 28 or 37 °C in a humidified atmosphere containing 5% CO_2.

Standard microbial strains used in this study (as listed in Table 1) were purchased from the China General Microbiological Culture Collection Center (CGMCC, https://www.cgmcc.net/). Clinically isolated multidrug-resistant (MDR) strains, including *A. baumannii* (QZ18050 and QZ18055), *Pseudomonas aeruginosa* (QZ19121 and QZ19122), and methicillin-resistant *S. aureus* (MRSA, QZ19130, and QZ19134), were obtained from the clinical strain repository of the Second Affiliated Hospital of Fujian Medical University, Quanzhou.

Sequence Analysis, Cloning, and Expression Profiling

A high-throughput AMP screening pipeline previously established by our laboratory was employed to identify candidate AMP precursor genes from uncharacterized transcripts based on transcriptomic data derived from *E. tarda*-challenged *B. pectinirostris*. Sequence identity analysis was conducted using the online BLAST tools available at the National Center for Biotechnology Information (NCBI; http://www.ncbi.nlm.nih.gov). The physicochemical properties of the predicted proteins were analyzed using the ProtParam tool (https://web.expasy.org/protparam/) and HeliQuest (https://heliquest.ipmc.cnrs.fr/cgi-bin/ComputParams.py). Tertiary structures of the proteins were predicted using AlphaFold (https://github.com/deepmind/alphafold) and visualized with PyMOL (https://www.pymol.org). Chemical structures of peptide candidates were constructed using ChemDraw (https://www.perkinelmer.com/category/chemdraw). Multiple sequence alignments were performed using the ClustalW algorithm implemented in MEGA 11. A phylogenetic tree was constructed using the Neighbor-Joining (NJ) method based on the Kimura 2-parameter model, and node reliability was assessed with 1,000 bootstrap replicates. The alignment results, integrated with predicted secondary structure information, were visualized using ESPript 3.0 (https://espript.ibcp.fr/ESPript/ESPript/). All homologous sequences used for phylogenetic and alignment analyses were retrieved from GenBank, and the corresponding sequence files are provided in the Supporting Information.

Total RNA was extracted from various tissues using TRIzol Reagent (Invitrogen, U.K.) following the manufacturer's protocol. RNA concentration and purity were evaluated with an Agilent 2100 Bioanalyzer (Agilent Technologies), and integrity was confirmed by 1.0% agarose gel electrophoresis. Equal quantities of RNA from different tissues were pooled for downstream cDNA synthesis. First-strand cDNA was synthesized using the SMARTer RACE 5′/3′ Kit (Clontech), and full-length cDNAs were amplified using LA Taq DNA polymerase (Takara, Japan), a high-fidelity enzyme optimized for long-fragment amplification. The resulting PCR products were ligated into the pMD18-T vector (Takara, China), transformed into *E. coli*, and subjected to bidirectional Sanger sequencing by Sangon Biotech Co., Ltd. (Shanghai, China).

Quantitative real-time PCR (qPCR) was conducted to analyze tissue-specific distribution, and the expression changes following pathogen infection. cDNA synthesis was performed using the PrimeScript RT reagent kit with gDNA Eraser (Takara, Japan), according to the manufacturer's instructions. For tissue distribution analysis, absolute quantification was performed based on standard curves derived from serially diluted PCR products. For expression profiling postchallenge, relative quantification was carried out using the $2^{-\Delta\Delta Ct}$ method. To ensure accurate normalization, the expression stability of four candidate reference genes—rpl8, 18s rRNA, gapdh, and β-actin—was evaluated using the RefFinder tool (https://blooge.cn/RefFinder/), which integrates multiple algorithms (geNorm, NormFinder, BestKeeper, and the comparative ΔCt method). Among the candidates, rpl8 was identified as the most stable and was selected as the internal control (see Supporting Figure 3 for stability assessment). qPCR assays were performed using the Bio-Rad CFX96 Real-Time PCR Detection System with an SYBR Premix Ex Taq II instrument (Takara, Japan). Each 20 μL reaction contained 10 μL of SYBR mix, 0.4 μL each of forward and reverse primers (10 μM), 2 μL of cDNA, and 7.2 μL of nuclease-free water. The thermal cycling conditions were as follows: initial denaturation at 95 °C for 30 s, followed by 40 cycles of 95 °C for 5 s and 60 °C for 30 s. A melting curve analysis was conducted to verify amplification specificity. All reactions were run in technical triplicates, and no-template controls were included in each assay.

Synthesis of the Predicted AMP

The full-length cDNA sequence of Boleokidin, from which the putative antimicrobial region was identified, has been deposited in GenBank under accession number OR195699. Based on this sequence, the truncated peptide Boleokidin$_{39-61}$ (H-VLGLVQFIHKLRVVKKSMKKKKM-OH) was chemically synthesized by Genscript (Nanjing, China). The synthesized peptide exhibited a purity of 96.8%, as determined by RP-HPLC, and its observed molecular weight (2739.0 Da) was confirmed by ESI-MS (quality certificates are provided in the Supporting Information). Lyophilized peptide samples were stored at −20 °C until further use.

Antimicrobial Activity Assay

The antimicrobial activity of the peptides was evaluated using the broth microdilution method, as specified in the Clinical and Laboratory Standards Institute (CLSI) guidelines. Bacterial cells were harvested

https://doi.org/10.1021/acs.jnatprod.5c01507
J. Nat. Prod. XXXX, XXX, XXX−XXX

during the logarithmic growth phase, washed, and resuspended in Mueller-Hinton Broth (MHB; Oxoid, U.K.) to a final concentration of 1×10^6 CFU/mL.[57,58] Peptides were prepared at appropriate concentrations and mixed with the bacterial suspension in a 1:1 volume ratio, yielding a final reaction volume of 100 μL per well. The mixtures were then transferred into 96-well polystyrene flat-bottomed microplates (NEST, China), resulting in final peptide concentrations ranging from 1.5 to 96 μM. Wells containing only bacteria served as negative controls, and wells containing effective antibiotics were included as positive controls. The plates were incubated under temperature-controlled conditions according to the optimal growth temperature of each bacterial strain for 24 h. The minimum inhibitory concentration (MIC) was determined by visual inspection as the lowest peptide concentration that completely inhibited visible bacterial growth. To determine the minimum bactericidal concentration (MBC), aliquots from wells showing no visible growth were plated on the agar and incubated to assess colony formation. The MBC was defined as the lowest concentration at which no colonies were observed. Each assay was performed with three technical replicates and was repeated in three independent experiments.

Time-Kill Kinetics Assay

The bactericidal kinetics of the peptides were evaluated against *A. baumannii* using a time-kill assay. Bacterial cells were harvested during the logarithmic growth phase, washed, and diluted in MHB to a final concentration of approximately 1×10^6 CFU/mL. The bacterial suspension was then incubated with peptides at concentrations equivalent to 1 × MBC and 2× MBC. At designated time points, aliquots were withdrawn, serially diluted, and plated on nutrient agar to determine the number of viable colonies. Colony counts were performed after incubation overnight under optimal conditions. The percentage of surviving bacteria at each time point was calculated using the following formula: Recovered CFU (% of initial) = (CFU at time point/CFU at 0 h) × 100%. All experiments were performed in triplicate, and each assay was independently repeated three times to ensure reproducibility.

Salt Tolerance Assay

To evaluate the salt tolerance of peptide activity over time, *A. baumannii* was coincubated with peptides (at 1× MBC) in the presence of varying concentrations of NaCl (0−160 mM). The peptide−bacteria mixtures were transferred into 96-well microplates and incubated overnight at 37 °C in a microplate reader equipped with a temperature-controlled chamber. Optical density at 600 nm (OD_{600}) was measured at regular intervals to monitor the bacterial growth kinetics under salt stress. All experiments were performed in triplicate, and each assay was independently repeated three times to ensure reproducibility.

Bacterial Membrane Permeability Assay

Bacterial inner membrane permeability was assessed using the LIVE/DEAD BacLight Bacterial Viability Kit (Thermo Fisher Scientific). Log-phase cultures of *A. baumannii* and *S. aureus* were harvested, washed, and resuspended in 10 mM sodium phosphate buffer (NaPB, pH 7.4) to a final concentration of 1×10^7 CFU/mL. Bacterial suspensions were incubated with peptides at a final concentration of 1 × MBC at 37 °C for 30 min. After incubation, the cells were washed twice with NaPB to remove residual peptides. The samples were then stained with SYTO 9 and propidium iodide (PI) according to the manufacturer's instructions and incubated at room temperature in the dark for 15 min. Stained bacteria were imaged and analyzed using confocal laser scanning microscopy (CLSM, Zeiss LSM780, Germany). Membrane-compromised (dead) cells exhibited red fluorescence due to PI uptake, while all cells (both live and dead) showed green fluorescence from SYTO 9 staining.

To further assess the outer membrane disruption in Gram-negative bacteria, we performed an *N*-phenyl-1-naphthylamine (NPN, Sigma, Germany) uptake assay was performed. Log-phase *A. baumannii* cells were suspended in HEPES buffer (pH 7.4, 5 mM glucose) to a final concentration of approximately 1×10^8 CFU/mL. NPN (10 μM final concentration) was added, and the mixture was transferred to a black 96-well plate (NUNC, Denmark). Fluorescence (Ex/Em = 350/420 nm) was recorded using a microplate reader until baseline stability was achieved. Then, $Boleokidin_{39-61}$ at different concentrations (3 μM and 6 μM) was introduced. Milli-Q water and polymyxin B (1 μg/mL) were used as negative and positive controls, respectively. Fluorescence intensities were measured at 2 min intervals for each condition. Three technical replicates were included per group, and the assay was independently repeated three times.

Scanning Electron Microscopy (SEM) Observation

To observe the morphological changes in bacteria and fungal spores after peptide treatment, SEM was performed. Log-phase bacterial cultures or fungal spores were collected, washed, and resuspended in 10 mM sodium phosphate buffer (NaPB, pH 7.4) to a final concentration of 1×10^7 CFU/mL. The microbial suspensions were incubated with peptides at a final concentration of 1× minimum bactericidal concentration (MBC) at 37 °C for 30 min. After treatment, the cells were collected by centrifugation at 5000×*g* for 5 min and fixed overnight at 4 °C in 2.5% (v/v) glutaraldehyde (Sigma, Germany). The samples were washed three times with NaPB and were resuspended in a small volume (10 μL) of NaPB to concentrate the cells. A 10 μL aliquot of each suspension was dropped onto poly-L-lysine-coated slides (0.5 × 0.8 cm^2) and allowed to adsorb on ice for 30 min. Excess liquid was gently removed with a filter paper. The adhered microbial cells were then dehydrated through a graded ethanol series (e.g., 30%, 50%, 70%, 90%, and 100%) and were dried using a critical point dryer (JFC-1600, Jeol GmbH, Germany). The dried specimens were mounted, sputter-coated with gold, and observed under a scanning electron microscope (FEI Quanta 650 FEG) for morphological analysis.

Intracellular Reactive Oxygen Species (ROS) Detection

Intracellular ROS levels in bacteria were measured using a commercial detection kit containing the fluorescent probe 2′,7′-dichlorodihydrofluorescein diacetate (DCFH-DA), purchased from the Nanjing Jiancheng Bioengineering Institute (China).

Bacterial cells were harvested during the logarithmic growth phase, washed, and resuspended in phosphate-buffered saline (PBS) to a final concentration of 1×10^8 CFU/mL. The bacterial suspension was then incubated with various concentrations of peptides for 30 min at 37 °C. The antimicrobial peptide LL-37 was used as a positive control. Following incubation, the cells were washed three times with PBS to remove excess peptides. The washed cells were then incubated with DCFH-DA at a final concentration of 10 μM for 30 min at 37 °C in the dark. Fluorescence intensity, indicative of ROS production, was measured using a microplate reader (excitation/emission: typically 488/525 nm). Each experimental condition was tested with five technical replicates, and the entire experiment was independently repeated 3 times.

To further explore the contribution of ROS to the bactericidal mechanism of $Boleokidin_{39-61}$, thiourea, a well-characterized ROS scavenger, was used as an intervention. Log-phase *A. baumannii* and *S. aureus* cells were preincubated with 100 mM thiourea for 10 min at 37 °C prior to peptide exposure. $Boleokidin_{39-61}$ was then added at 1 × MBC, and the mixture was incubated for 1 h. Samples were divided for two assays: (i) ROS detection using DCFH-DA staining as described above and (ii) colony-forming unit (CFU) enumeration by serial dilution and plating to determine viable bacterial counts after thiourea pretreatment. This approach allowed assessment of both intracellular ROS levels and the potential protective effect of thiourea against peptide-mediated bacterial killing. All experiments were independently repeated at least 3 times.

Induction of Bacterial Resistance Under Long-Term AMP Exposure

To assess the potential of long-term peptide exposure to induce bacterial resistance, a serial passaging assay was conducted over a 48-day period using *A. baumannii* and *S. aureus*.

For *A. baumannii*, the tested agents included the target peptide, LL-37, tigecycline, and gentamicin. For *S. aureus*, the tested agents included the target peptide, LL-37, ampicillin, and vancomycin. Each day, the MIC of each antimicrobial agent was determined using the broth microdilution method according to standard protocols. Following MIC

https://doi.org/10.1021/acs.jnatprod.5c01507
J. Nat. Prod. XXXX, XXX, XXX−XXX

determination, the bacterial culture from the highest concentration well showing visible growth (i.e., sub-MIC condition) was diluted 1:1000 in fresh MHB and used to inoculate a new 96-well microdilution plate containing a fresh 2-fold dilution series of the corresponding antimicrobial agent. This process was repeated daily for 48 consecutive days. MIC values were recorded each day to monitor the development of the resistance. Each experimental condition was performed in triplicate and repeated independently 3 times to ensure reproducibility.

Cytotoxicity and Hemolytic Activity Assays

The cytotoxic effects of peptides on cells were evaluated by using the MTS assay. Cells were seeded into 96-well tissue culture plates (Thermo Fisher Scientific) at a density of 1×10^4 cells per well and incubated overnight at 28 °C/37 °C in a humidified incubator with 5% CO_2. The following day, the culture medium was replaced with fresh medium containing different concentrations of peptides (ranging from 0 to 96 μM). Wells containing a medium without peptide served as the negative control, while melittin-treated wells served as the positive control. After 24 h of incubation, cell viability was measured using the CellTiter 96 AQueous One Solution Cell Proliferation Assay Kit (Promega), following the manufacturer's instructions. Each treatment was tested in five technical replicates, and the entire assay was independently repeated 3 times.

Hemolytic activity was assessed by using freshly isolated mouse red blood cells (RBCs). Whole blood was centrifuged at 500×*g* for 3 min, and the RBCs were washed repeatedly with 0.9% saline until the supernatant was clear. The washed RBCs were then resuspended to a final concentration of 4% (v/v) in saline. In a 96-well microplate, equal volumes of RBC suspension and peptide solutions at various concentrations were mixed and incubated at 37 °C for 1 h. After incubation, the samples were centrifuged at 4000 rpm for 3 min, and the supernatant was transferred to a new 96-well plate. Hemoglobin release was quantified by measuring the absorbance at 540 nm using a microplate reader. 0.9% saline was used as the negative control (no hemolysis), and 0.1% Triton X-100 in 0.9% saline was used as the positive control (100% hemolysis). The percentage of hemolysis was calculated by using the following formula: Hemolytic activity (%) = $[(A_{540}$ of test sample $- A_{540}$ of negative control$)/(A_{540}$ of positive control $- A_{540}$ of negative control$)] \times 100\%$. Each condition was tested in five technical replicates and repeated in three independent experiments.

In Vivo Protective Efficacy of an AMP in a Zebrafish Infection Model

To evaluate the in vivo immunoprotective effect of the peptide, a zebrafish (*D. rerio*) infection model was established by using *A. hydrophila*. A total of 160 adult zebrafish were randomly divided into four groups (n = 40 per group): (1) uninfected and PBS-injected control group, (2) uninfected and peptide-injected group, (3) infected but untreated group, and (4) infected and peptide-treated group.

At 0 h, fish in the infected groups were intraperitoneally injected with 8.8 μL of *A. hydrophila* suspension (approximately 7×10^8 CFU/mL, prepared in PBS), while the uninfected groups received the same volume of sterile PBS. All injections were performed using a Hamilton PB600-1 repeating dispenser (Hamilton, Supporting Figure 4), which delivers this fixed volume per actuation. One hour postinfection, the peptide-treated group and the uninfected + peptide group were injected with the same fixed volume (8.8 μL) of peptide solution (1.5 mg/mL), whereas the other two groups were injected with an equivalent volume of PBS. Fish were monitored for mortality over a 48 h period, and survival data were recorded. Kaplan−Meier survival curves were generated by using GraphPad Prism software. The statistical significance was determined by the log-rank (Mantel-Cox) test, and the Cox proportional hazards model was applied to quantify treatment effect size.

At the end of the experiment, liver tissues from each group were aseptically collected, weighed, and homogenized in sterile PBS. Bacterial loads were determined by plating serial dilutions of the homogenates onto the *A. hydrophila*-selective agar. To assess immune responses, total RNA was extracted from liver tissues, and the expression of genes related to inflammatory cytokines, antimicrobial peptides, and Toll-like receptors (TLRs) was analyzed via relative quantitative real-time PCR. Additionally, reactive oxygen species (ROS) levels and myeloperoxidase (MPO) activity in liver samples were measured using commercial detection kits from Nanjing Jiancheng Bioengineering Institute (China) and Solarbio (China), respectively, according to the manufacturers' instructions. All quantitative data were normalized against the uninfected PBS control group. Specifically, for each parameter, the values of all experimental groups were divided by the average value of the uninfected control group, and expressed as fold changes. This normalization was performed uniformly across all data sets to allow consistent and comparable evaluation of infection-induced effects and peptide-mediated modulation relative to baseline conditions.

Evaluation of Safety and Acute Toxicity of Boleokidin$_{39-61}$ in Mice

All mice experiments were conducted in accordance with institutional guidelines and were approved by the Ethics Committee of the Xiamen University Laboratory Animal Center (Protocol No. XMU-LAC20260002). Female BALB/c mice aged 6−8 weeks were purchased from Beijing Weitong Lihua Experimental Animal Technical Co., Ltd. (Beijing, China). The acute toxicity evaluation followed previously reported methods with minor adjustments.[59] Fifteen mice were used in total, including a PBS control group and two treatment groups receiving intraperitoneal injections of Boleokidin$_{39-61}$ or Polymyxin B (10 mg/kg), with five mice per group (n = 5). Mice were monitored for 5 days, and their activity, posture, coat condition, respiration, food intake, and body weight were recorded. Clinical manifestations were categorized as normal, mild illness, severe illness, or death, and mice exhibiting severe illness were euthanized according to ethical guidelines. Liver and kidney tissues were collected at the end of the observation period for histopathological analysis.

For the therapeutic efficacy study, an acute peritonitis model was established following previously described protocols with minor adjustments.[60] Mice were anesthetized with 2.5% Avertin and intraperitoneally injected with 100 μL of *E. coli* ATCC 1.2385 suspension containing 1×10^8 CFU; uninfected controls received PBS. One hour postinfection, mice were treated intraperitoneally with PBS, Boleokidin$_{39-61}$ (10 mg/kg), or Polymyxin B (10 mg/kg). Each experimental group also consisted of five mice (n = 5). Mice were monitored for 24 h before sampling, after which liver tissues were collected for viable bacterial counting and for the quantification of inflammatory cytokines (TNF-α, IL-1β, IL-6) by qPCR.

Statistical Analysis

All experimental data were analyzed using SPSS 18.0 software (IBM). Data are presented as the mean ± standard deviation (SD) from at least three independent experiments. For comparisons between two groups, statistical significance was assessed using a two-tailed Student t test, with $p < 0.05$ considered statistically significant. For multiple group comparisons, one-way analysis of variance (ANOVA) followed by post hoc tests was used. Statistically significant differences among groups were denoted by different lowercase letters (e.g., *a*, *b*, *c*, and *d*).

■ ASSOCIATED CONTENT

Data Availability Statement

No data were used for the research described in the article.

Supporting Information

The Supporting Information is available free of charge at https://pubs.acs.org/doi/10.1021/acs.jnatprod.5c01507.

GenBank-derived homologous sequences used for phylogenetic analysis; along with quality certificates for the synthesized peptide; including the Certificate of Analysis; RP-HPLC chromatogram; and ESI-MS spectrum (ZIP)

Full-length Boleokidin gene sequence; microscopy images showing inhibition of fungal spore germination;

https://doi.org/10.1021/acs.jnatprod.5c01507
J. Nat. Prod. XXXX, XXX, XXX−XXX

NPN outer membrane permeability assay results; reference gene stability analysis outputs; and an image with product information for the Hamilton PB600-1 dispenser used in zebrafish injections (PDF)

AUTHOR INFORMATION

Corresponding Authors

Fangyi Chen − *State Key Laboratory of Marine Environmental Science, College of Ocean & Earth Sciences, Xiamen University, Xiamen 361102 Fujian, China; State-Province Joint Engineering Laboratory of Marine Bioproducts and Technology, College of Ocean & Earth Sciences, Xiamen University, Xiamen 361102 Fujian, China; Marine Biological Antimicrobial Peptides Industry Research Institute, Fujian Ocean Innovation Center, Xiamen 361102, China;* orcid.org/0000-0001-5714-1339; Email: chenfangyi@xmu.edu.cn

Ke-Jian Wang − *State Key Laboratory of Marine Environmental Science, College of Ocean & Earth Sciences, Xiamen University, Xiamen 361102 Fujian, China; State-Province Joint Engineering Laboratory of Marine Bioproducts and Technology, College of Ocean & Earth Sciences, Xiamen University, Xiamen 361102 Fujian, China; Marine Biological Antimicrobial Peptides Industry Research Institute, Fujian Ocean Innovation Center, Xiamen 361102, China;* Email: wkjian@xmu.edu.cn

Authors

Yuqi Bai − *State Key Laboratory of Marine Environmental Science, College of Ocean & Earth Sciences, Xiamen University, Xiamen 361102 Fujian, China; State-Province Joint Engineering Laboratory of Marine Bioproducts and Technology, College of Ocean & Earth Sciences, Xiamen University, Xiamen 361102 Fujian, China*

Jingyuan Zhan − *State Key Laboratory of Marine Environmental Science, College of Ocean & Earth Sciences, Xiamen University, Xiamen 361102 Fujian, China; State-Province Joint Engineering Laboratory of Marine Bioproducts and Technology, College of Ocean & Earth Sciences, Xiamen University, Xiamen 361102 Fujian, China*

Weibin Zhang − *State Key Laboratory of Marine Environmental Science, College of Ocean & Earth Sciences, Xiamen University, Xiamen 361102 Fujian, China; State-Province Joint Engineering Laboratory of Marine Bioproducts and Technology, College of Ocean & Earth Sciences, Xiamen University, Xiamen 361102 Fujian, China*

Wenbin Zheng − *State Key Laboratory of Marine Environmental Science, College of Ocean & Earth Sciences, Xiamen University, Xiamen 361102 Fujian, China; State-Province Joint Engineering Laboratory of Marine Bioproducts and Technology, College of Ocean & Earth Sciences, Xiamen University, Xiamen 361102 Fujian, China*

Complete contact information is available at: https://pubs.acs.org/10.1021/acs.jnatprod.5c01507

Author Contributions

[1]Y.B. and J.Z.: co-first authors. Y.B. and J.Z.: investigation, methodology, data curation, formal analysis, visualization, writing—original draft. W.Z.: investigation, methodology. W.Z.: investigation. F.C.: writing—review and editing, conceptualization, supervision, project administration, funding acquisition. K.-J.W.: writing—review and editing, conceptualization, supervision, project administration, funding acquisition.

Notes

The authors declare no competing financial interest.

ACKNOWLEDGMENTS

This work was supported by the National Natural Science Foundation of China (Grant No. 42376089), the China Postdoctoral Science Foundation (Grant No. 2025M770855), and the Postdoctoral Fellowship Program of CPSF (Grant No. GZC20250580). Additional support was provided by the Fujian Ocean and Fisheries Bureau (Grant No. FJHYF-L-2025-13), Fujian Province Industry-Academia Collaboration Project (Grant No. 2025N5001), the Xiamen Ocean Development Bureau (Grant No. 22CZP002HJ08), and the Pingtan Research Institute of Xiamen University (Grant No. Z20220743).

REFERENCES

(1) Salam, M. A.; Al-Amin, M. Y.; Salam, M. T.; et al. Antimicrobial resistance: a growing serious threat for global public health. *Healthcare* **2023**, *11* (13), No. 1946, DOI: 10.3390/healthcare11131946.

(2) Hossain, A.; Habibullah-Al-Mamun, M.; Nagano, I.; et al. Antibiotics, antibiotic-resistant bacteria, and resistance genes in aquaculture: risks, current concern, and future thinking. *Environ. Sci. Pollut. Res.* **2022**, *29* (8), 11054−11075.

(3) Bristol, N. *The US Government and Antimicrobial Resistance*; JSTOR, 2020.

(4) Pepi, M.; Focardi, S. Antibiotic-resistant bacteria in aquaculture and climate change: a challenge for health in the mediterranean area. *Int. J. Environ. Res. Public Health* **2021**, *18* (11), No. 5723, DOI: 10.3390/ijerph18115723.

(5) Singha, B.; Singh, V.; Soni, V. Alternative therapeutics to control antimicrobial resistance: a general perspective. *Front. Drug Discovery* **2024**, *4*, No. 1385460.

(6) Büyükkiraz, M. E.; Kesmen, Z. Antimicrobial peptides (AMPs): a promising class of antimicrobial compounds. *J. Appl. Microbiol.* **2022**, *132* (3), 1573−1596.

(7) Pasupuleti, M.; Schmidtchen, A.; Malmsten, M. Antimicrobial peptides: key components of the innate immune system. *Crit. Rev. Biotechnol.* **2012**, *32* (2), 143−171.

(8) Chen, N.; Jiang, C. Antimicrobial peptides: structure, mechanism, and modification. *Eur. J. Med. Chem.* **2023**, *255*, No. 115377.

(9) K, R. G.; Narasingappa, R. B.; Vyas, G. V. Unveiling mechanisms of antimicrobial peptide: actions beyond the membranes disruption. *Heliyon* **2024**, *10* (19), No. e38079.

(10) Lyu, Z.; Yang, P.; Lei, J.; Zhao, J. Biological function of antimicrobial peptides on suppressing pathogens and improving host immunity. *Antibiotics* **2023**, *12* (6), No. 1037, DOI: 10.3390/antibiotics12061037.

(11) Mahlapuu, M.; Bjorn, C.; Ekblom, J. Antimicrobial peptides as therapeutic agents: opportunities and challenges. *Crit. Rev. Biotechnol.* **2020**, *40* (7), 978−992.

(12) Divyashree, M.; Mani, M. K.; Reddy, D.; et al. Clinical applications of antimicrobial peptides (AMPs): where do we stand now? *Protein Peptide Lett.* **2020**, *27* (2), 120−134.

(13) Macedo, M. W. F. S.; Cunha, N. B. d.; Carneiro, J. A.; et al. Marine organisms as a rich source of biologically active peptides. *Front. Mar. Sci.* **2021**, *8*, No. 667764.

(14) Ishimatsu, A.; Mai, H. V.; Martin, K. L. M. Patterns of fish reproduction at the interface between air and water. *Integr. Comp. Biol.* **2018**, *58* (6), 1064−1085.

(15) Sayer, M. D. J. Adaptations of amphibious fish for surviving life out of water. *Fish Fish.* **2005**, *6* (3), 186−211.

(16) Wang, G.; Li, X.; Wang, Z. APD3: the antimicrobial peptide database as a tool for research and education. *Nucleic Acids Res.* **2016**, *44* (D1), D1087−D1093, DOI: 10.1093/nar/gkv1278.

(17) Lithgow, T.; Stubenrauch, C. J.; Stumpf, M. P. Surveying membrane landscapes: a new look at the bacterial cell surface. *Nat. Rev. Microbiol.* **2023**, *21* (8), 502−518.
(18) Yin, L. M.; Edwards, M. A.; Li, J.; et al. Roles of hydrophobicity and charge distribution of cationic antimicrobial peptides in peptide-membrane interactions. *J. Biol. Chem.* **2012**, *287* (10), 7738−7745.
(19) Tan, R.; Wang, M.; Xu, H.; et al. Improving the activity of antimicrobial peptides against aquatic pathogen bacteria by amino acid substitutions and changing the ratio of hydrophobic residues. *Front. Microbiol.* **2021**, *12*, No. 773076.
(20) Gawde, U.; Chakraborty, S.; Waghu, F. H.; et al. $CAMP_{R4}$: a database of natural and synthetic antimicrobial peptides. *Nucleic Acids Res.* **2023**, *51* (D1), D377−D383, DOI: 10.1093/nar/gkac933.
(21) Zhong, A.; Yan, X. Erythropoiesis in teleost fishes: the fantastic biological process. *Rev. Aquacult.* **2025**, *17* (1), No. e12960.
(22) Wang, J.; Su, B.; Dunham, R. A. Genome-wide identification of catfish antimicrobial peptides: a new perspective to enhance fish disease resistance. *Rev. Aquacult.* **2022**, *14* (4), 2002−2022.
(23) Rodrigues, P. N.; Vázquez-Dorado, S.; Neves, J. V.; Wilson, J. M. Dual function of fish hepcidin: response to experimental iron overload and bacterial infection in sea bass (*Dicentrarchus labrax*). *Dev. Comp. Immunol.* **2006**, *30* (12), 1156−1167.
(24) Muniz, L. R.; Knosp, C.; Yeretssian, G. Intestinal antimicrobial peptides during homeostasis, infection, and disease. *Front. Immunol.* **2012**, *3*, No. 310.
(25) Meng, X.-Z.; Duan, Y.; Bai, Y.; et al. The antimicrobial peptide $Sparamosin_{26-54}$ exhibits antiviral activity against three aquatic enveloped viruses through lipid-binding-mediated virus lysis. *Aquaculture* **2024**, *592*, No. 741160.
(26) Wang, B.; Lin, P.; Zhong, Y.; et al. Explainable deep learning and virtual evolution identifies antimicrobial peptides with activity against multidrug-resistant human pathogens. *Nat. Microbiol.* **2025**, *10* (2), 332−347.
(27) Becknell, B.; Schwaderer, A.; Hains, D. S.; Spencer, J. D. Amplifying renal immunity: the role of antimicrobial peptides in pyelonephritis. *Nat. Rev. Nephrol.* **2015**, *11* (11), 642−655.
(28) Udroiu, I.; Sgura, A. The phylogeny of the spleen. *Q. Rev. Biol.* **2017**, *92* (4), 411−443.
(29) Zhu, W.; Su, J. Immune functions of phagocytic blood cells in teleost. *Rev. Aquacult.* **2022**, *14* (2), 630−646.
(30) Wilson, D. N.; Hauryliuk, V.; Atkinson, G. C.; O'Neill, A. J. Target protection as a key antibiotic resistance mechanism. *Nat. Rev. Microbiol.* **2020**, *18* (11), 637−648.
(31) Gow, N. A. R.; Lenardon, M. D. Architecture of the dynamic fungal cell wall. *Nat. Rev. Microbiol.* **2023**, *21* (4), 248−259.
(32) Yu, W.; Guo, X.; Li, Q.; et al. Revolutionizing antimicrobial biomaterials: integrating an enzyme degradation-resistant sequence into self-assembled nanosystems to overcome stability limitations of peptide-based drugs. *Adv. Fiber Mater.* **2024**, *6* (4), 1188−1211.
(33) Bai, Y.; Zhang, W.; Zheng, W.; et al. A 14-amino acid cationic peptide $Bolespleenin_{334-347}$ from the marine fish mudskipper *Boleophthalmus pectinirostris* exhibiting potent antimicrobial activity and therapeutic potential. *Biochem. Pharmacol.* **2024**, *226*, No. 116344.
(34) Yin, L. M.; Edwards, M. A.; Li, J.; et al. Roles of hydrophobicity and charge distribution of cationic antimicrobial peptides in peptide-membrane interactions. *J. Biol. Chem.* **2012**, *287* (10), 7738−7745.
(35) Rojas, E. R.; Billings, G.; Odermatt, P. D.; et al. The outer membrane is an essential load-bearing element in Gram-negative bacteria. *Nature* **2018**, *559* (7715), 617−621.
(36) Percy, M. G.; Gründling, A. Lipoteichoic acid synthesis and function in Gram-positive bacteria. *Annu. Rev. Microbiol.* **2014**, *68* (1), 81−100.
(37) Kabelka, I.; Vácha, R. Advances in molecular understanding of α-helical membrane-active peptides. *Acc. Chem. Res.* **2021**, *54* (9), 2196−2204.
(38) Sani, M.-A.; Separovic, F. How membrane-active peptides get into lipid membranes. *Acc. Chem. Res.* **2016**, *49* (6), 1130−1138.
(39) Zhang, W.; An, Z.; Bai, Y.; et al. A novel antimicrobial peptide $Scyreptin_{1-30}$ from *Scylla paramamosain* exhibiting potential therapy of *Pseudomonas aeruginosa* early infection in a mouse burn wound model. *Biochem. Pharmacol.* **2023**, *218*, No. 115917.
(40) Melo, M. N.; Ferre, R.; Castanho, M. A. Antimicrobial peptides: linking partition, activity and high membrane-bound concentrations. *Nat. Rev. Microbiol.* **2009**, *7* (3), 245−250.
(41) Wang, X.; Zhao, X.; Malik, M.; Drlica, K. Contribution of reactive oxygen species to pathways of quinolone-mediated bacterial cell death. *J. Antimicrob. Chemother.* **2010**, *65* (3), 520−524.
(42) Bastos, M. L. C.; Ferreira, G. G.; Kosmiscky, I. O.; et al. What do we know about *Staphylococcus aureus* and oxidative stress? Resistance, virulence, new targets, and therapeutic alternatives. *Toxics* **2025**, *13* (5), No. 390, DOI: 10.3390/toxics13050390.
(43) Rowe, S. E.; Wagner, N. J.; Li, L.; et al. Reactive oxygen species induce antibiotic tolerance during systemic *Staphylococcus aureus* infection. *Nat. Microbiol.* **2020**, *5* (2), 282−290.
(44) Daniels, R.; Vanderleyden, J.; Michiels, J. Quorum sensing and swarming migration in bacteria. *FEMS Microbiol. Rev.* **2004**, *28* (3), 261−289.
(45) Laventie, B.-J.; Jenal, U. Surface sensing and adaptation in bacteria. *Annu. Rev. Microbiol.* **2020**, *74* (1), 735−760.
(46) Wang, J.; Li, G.; Yin, H.; An, T. Bacterial response mechanism during biofilm growth on different metal material substrates: EPS characteristics, oxidative stress and molecular regulatory network analysis. *Environ. Res.* **2020**, *185*, No. 109451.
(47) Theuretzbacher, U.; Bush, K.; Harbarth, S.; et al. Critical analysis of antibacterial agents in clinical development. *Nat. Rev. Microbiol.* **2020**, *18* (5), 286−298.
(48) Huang, Y.; Huang, J.; Chen, Y. Alpha-helical cationic antimicrobial peptides: relationships of structure and function. *Protein Cell* **2010**, *1* (2), 143−152.
(49) Trubenová, B.; Roizman, D.; Moter, A.; et al. Population genetics, biofilm recalcitrance, and antibiotic resistance evolution. *Trends Microbiol.* **2022**, *30* (9), 841−852.
(50) Travkova, O. G.; Moehwald, H.; Brezesinski, G. The interaction of antimicrobial peptides with membranes. *Adv. Colloid Interface Sci.* **2017**, *247*, 521−532.
(51) Hollmann, A.; Martínez, M.; Noguera, M. E.; et al. Role of amphipathicity and hydrophobicity in the balance between hemolysis and peptide−membrane interactions of three related antimicrobial peptides. *Colloids Surf., B* **2016**, *141*, 528−536.
(52) Zhuang, L.; Kim, J.; Adam, R. M.; et al. Cholesterol targeting alters lipid raft composition and cell survival in prostate cancer cells and xenografts. *J. Clin. Invest.* **2005**, *115* (4), 959−968.
(53) Saraceni, P. R.; Romero, A.; Figueras, A.; Novoa, B. Establishment of infection models in zebrafish larvae (*Danio rerio*) to study the pathogenesis of *Aeromonas hydrophila*. *Front. Microbiol.* **2016**, *7*, No. 1219.
(54) Zhu, L.-y.; Nie, L.; Zhu, G.; et al. Advances in research of fish immune-relevant genes: a comparative overview of innate and adaptive immunity in teleosts. *Dev. Comp. Immunol.* **2013**, *39* (1−2), 39−62.
(55) Abdelraouf, K.; Braggs, K. H.; Yin, T.; et al. Characterization of polymyxin B-induced nephrotoxicity: implications for dosing regimen design. *Antimicrob. Agents Chemother.* **2012**, *56* (9), 4625−4629.
(56) Kagi, T.; Naganuma, R.; Inoue, A.; et al. The polypeptide antibiotic polymyxin B acts as a pro-inflammatory irritant by preferentially targeting macrophages. *J. Antibiotics* **2022**, *75* (1), 29−39.
(57) Smith, K. P.; Kirby, J. E. The inoculum effect in the era of multidrug resistance: minor differences in inoculum have dramatic effect on MIC determination. *Antimicrob. Agents Chemother.* **2018**, *62* (8), No. 10-1128, DOI: 10.1128/AAC.00433-18.
(58) Cockerill, F. R. Methods for dilution antimicrobial susceptibility tests for bacteria that grow aerobically: approved standard. 2012.
(59) Ouyang, X.; Li, B.; Yang, Y.; et al. Improving the antimicrobial performance of amphiphilic cationic antimicrobial peptides using glutamic acid full-scan and positive charge compensation strategies. *J. Med. Chem.* **2022**, *65* (20), 13833−13851.
(60) Zhong, C.; Zhang, F.; Yao, J.; et al. Antimicrobial peptides with symmetric structures against multidrug-resistant bacteria while

https://doi.org/10.1021/acs.jnatprod.5c01507
J. Nat. Prod. XXXX, XXX, XXX−XXX

alleviating antimicrobial resistance. *Biochem. Pharmacol.* **2021**, *186*, No. 114470.

https://doi.org/10.1021/acs.jnatprod.5c01507
J. Nat. Prod. XXXX, XXX, XXX−XXX